Can models robustly represent aerosol–convection interactions if their cloud microphysics is uncertain?

Bethan White[1], Edward Gryspeerdt[2], Philip Stier[1], Hugh Morrison[3], and Gregory Thompson[3]

[1]Atmospheric, Oceanic and Planetary Physics, University of Oxford, Oxford, UK
[2]Institute for Meteorology, Universität Leipzig, Leipzig, Germany
[3]National Center for Atmospheric Research, Boulder, Colorado

Correspondence to: Bethan White (bethan.white@physics.ox.ac.uk)

Abstract. This study investigates the hydrometeor development and response to cloud droplet number concentration (CDNC) perturbations in convection-permitting model configurations. We present results from a real-data simulation of deep convection in the Congo basin, an idealised supercell case, and a warm-rain large-eddy simulation (LES). In each case we compare two frequently used double-moment bulk microphysics schemes and investigate the response to CDNC perturbations. In the

5   Congo basin simulations both microphysics schemes have large positive biases in surface precipitation, frequency of high radar reflectivities and frequency of cold cloud compared to observations. In all cases, differences in the simulated cloud morphology and precipitation are found to be significantly greater between the microphysics schemes than due to CDNC perturbations within each scheme. Further, we show that the response of the hydrometeors to CDNC perturbations strongly differs not just between microphysics schemes but also between different cases of convection. Sensitivity tests show that the

10 representation of autoconversion is the dominant factor that drives differences in rain production between the microphysics schemes in the idealised precipitating shallow cumulus case and in a sub-region of the Congo basin simulations dominated by liquid-phase processes. In this region, rain mass is also shown to be relatively insensitive to the radiative effects of an overlying layer of ice-phase cloud. In the idealised supercell case, thermodynamic impacts on the storm system using different microphysics parameterisations can equal those due to aerosol effects. These results highlight the large uncertainty in cloud and

15 precipitation responses to aerosol in convection-permitting simulations and have important implications not just for modelling studies of aerosol–convection interaction. These results indicate the continuing need for tighter observational constraints of cloud processes and response to aerosol in a range of meteorological regimes.

1 Introduction

Deep convection has a significant influence on the state of the atmosphere and climate through shortwave and longwave ra-
20 diative interactions, heat transfer through the release of latent heat, global heat redistribution, and plays an important part in the hydrological cycle through the conversion of water vapour to precipitation. Aerosols can influence the properties of deep convection through their effect on cloud microphysics. By acting as cloud condensation nuclei (CCN), increased aerosol loading can lead to an increase in cloud droplet number concentration (CDNC) and subsequent reduction in cloud droplet size, which in turn has been hypothesised to suppress precipitation (Albrecht, 1989). Some theoretical (e.g. Rosenfeld et al., 2008;

Stevens and Feingold, 2009) and cloud (or cloud-system) resolving modelling studies (e.g. Khain et al., 2005; Tao et al., 2007; Lebo and Seinfeld, 2011, amongst many others) have suggested that under certain conditions, precipitation suppression in the liquid phase may lead to an invigoration of deep convection and subsequent enhancement of convective precipitation. The detection of positive correlations between satellite-observed aerosol optical depth (AOD) and precipitation or convective cloud properties (e.g. Koren et al., 2005; Gryspeerdt et al., 2014) might suggest observational evidence of convective invigoration by aerosols. However, factors such as meteorological covariation and retrieval errors may contribute to or even dominate such correlations (Zhang et al., 2005; Mauger and Norris, 2007; Chand et al., 2012; Gryspeerdt et al., 2014). Complex process interactions in ice and mixed-phase microphysics, along with coupling to surface and radiative feedbacks and dynamics over a range of spatiotemporal scales, means that understanding and quantifying aerosol impacts on deep convection remains a significant challenge (e.g. Noppel et al., 2010; Seifert et al., 2012; Tao et al., 2012).

Representing cloud microphysical processes, which occur on length scales of microns to millimetres, has always been a significant challenge for atmospheric models. Even in cloud-resolving models, horizontal grid lengths tend to be on the order of kilometres to a few hundred metres at best, and so it is impossible for such models to explicitly simulate microphysical processes. There is a long history of microphysical parameterisation (see Khain et al., 2015, for a comprehensive review), and microphysics schemes today tend to fall into one of two categories: bin models, in which the size distribution of each hydrometeor class is explicitly calculated (e.g. Feingold et al., 1994; Stevens et al., 1996; Khain et al., 2004), and bulk models, in which a size distribution function typically is used to represent each hydrometeor class and one (or several) moments of the size distribution function are calculated explicitly (e.g. Kessler, 1969; Lin et al., 1983; Rutledge and Hobbs, 1983; Thompson et al., 2004; Morrison et al., 2005; Thompson et al., 2008, amongst many others). Bulk models are therefore very computationally efficient compared to bin models (often by at least two orders of magnitude, Jiang et al., 2000), and are used as standard in many atmospheric modelling systems today. Whilst early bulk microphysics schemes were single moment only, a significant development has been predicting the second moment of the size distribution, usually number concentration (e.g. Meyers et al., 1997; Thompson et al., 2004; Morrison et al., 2005; Thompson et al., 2008). Indeed, although not widely used, three-moment schemes have been shown to further improve representations of large hail (Milbrandt and Yau, 2006; Loftus and Cotton, 2014)

Unlike liquid cloud and rain drops (well-described by spheres of constant density), ice particles have a wide range of densities and shapes, making the representation of ice-phase microphysics in parameterisations much more difficult than the liquid phase. Until recently, the approach in both bin (e.g. Khain et al., 2004) and bulk schemes (e.g. Meyers et al., 1997; Thompson et al., 2004; Morrison et al., 2005, etc.) was to partition ice particles into one of a fixed number of categories (e.g. cloud ice, snow, hail and graupel) each with its own specified density, shape distribution and physical parameters such as fall speeds. However, such partitioning oversimplifies the complex nature of ice-phase processes, requiring thresholds and parameters - often chosen on a relatively ad hoc basis - to determine the partitioning of ice particles into each category and for converting between categories. As such, it is unsurprising that simulations have been found to be highly sensitive to particle fall speeds and densities (e.g. McFarquhar et al., 2006), the description of dense precipitating ice as hail or graupel categories (e.g. Morrison

and Milbrandt, 2011; Bryan and Morrison, 2012), and changes in thresholds or rates for converting between ice categories (e.g. Morrison and Grabowski, 2008). Differences in ice-phase microphysics in bulk schemes have been shown to affect cloud biases especially at upper levels (Cintineo et al., 2014) and to affect ice–cloud–radiation feedbacks, with impacts on tropospheric stability, triggering of deep convection, and surface precipitation (Hong et al., 2009). Such limitations have led to the develop-
5   ment in more recent years of new representations of ice microphysics in bulk schemes, such as approaches which separately prognose ice mass mixing ratios grown by riming and vapour deposition (Morrison and Grabowski, 2008), where ice particle habit evolution is predicted by prognosing mixing ratios of ice crystal axes (Harrington et al., 2013), and where ice-phase particles are represented by several physical properties that evolve freely in time and space (Morrison and Milbrandt, 2015). Although these developments are relatively new, they have already been shown to improve simulations of observed squall lines
10 and orographic precipitation when compared to traditional two-moment bulk schemes (Morrison et al., 2015a).

Evaluations of microphysics schemes frequently involve comparison against observations of a real precipitation event (e.g. Morrison and Pinto, 2005). Often, multiple microphysics schemes are compared against each other and against observations (e.g. Morrison and Pinto, 2006; Gallus Jr. and Pfeifer, 2008; Rajeevan et al., 2010; Jankov et al., 2011). Another common
15 approach is to evaluate a single microphysics scheme against observations and then use different aerosol concentrations in the model to test the sensitivity of the observed storm to aerosol processes (e.g. van den Heever et al., 2006; Seifert et al., 2012). However, studies of different convective events in different regions, using different models with different microphysics schemes, often produce conflicting results on the nature of the storm repsonse to aerosol. Mesoscale studies of Florida convection found that cloud water mass, updraught strength and surface precipitation tend to increase with increased aerosol
20 concentration, while anvil areas decreased but contain greater condensate mass (van den Heever et al., 2006), whereas studies of summertime convective precipitation in Germany found that increased aerosol concentrations had a strong effect on cloud microphysical (and therefore radiative) properties but that the combined effects of microphysical and dynamical processes resulted in relatively little effect on surface precipitation (Seifert et al., 2012), similar to the findings of Thompson and Eidhammer (2014) in idealised and continental-scale simulations.

Detailed process modelling studies of aerosol–convection interactions often focus on the sensitivity of a single idealised model configuration (without large-scale meteorology or surface and radiative interactions) to perturbations, using either CCN spectra (e.g. Seifert and Beheng, 2006; Morrison and Grabowski, 2011) or CDNC values (e.g. Thompson et al., 2004; Morrison, 2012) as a proxy variable to test the sensitivity of the microphysics to aerosol. Many types of idealised models are used,
30 ranging from flow over a 2D mountain (e.g. Thompson et al., 2004), 2D cloud-system resolving studies of interacting convective clouds (e.g. Morrison and Grabowski, 2011), to 3D simulations of idealised supercell storms (e.g. Khain and Lynn, 2009; Lebo and Seinfeld, 2011; Morrison, 2012; Lebo et al., 2012). With such a wide range of model configurations, microphysics parameterisations (bin and bulk models are both frequently used in idealised studies of aerosol–convection interactions) and proxy variables used to represent aerosol processes, it is perhaps not surprising that a consistent response of idealised convec-
35 tion to aerosol has not been seen and indeed, due to regime-dependence, may not exist. Idealised flow over a 2D mountain

using CDNC values to represent aerosol amounts showed that cloud water content increased with CDNC, and drizzle content decreased (Thompson et al., 2004), while a similar study using an idealised supercell configuration found that differences in the accumulated surface precipitation and convective mass flux between polluted and pristine values of CDNC were very small (Morrison, 2012). In studies using modified CCN spectra to represent different levels of aerosol in a two-moment scheme, 2D

5 ensemble simulations of interacting convective clouds have found that although cloud top heights and anvil ice increase under polluted conditions, convection actually weakens slightly compared to pristine conditions (Morrison and Grabowski, 2011). However, similar 3D simulations also using a two-moment microphysics scheme have shown that for isolated convective cells, increased aerosol leads to reduced total precipitation and updraught velocity, while for multicell systems it leads to increased secondary convection, total precipitation and updraught velocities, whilst supercell systems are relatively insensitive to aerosol

10 (Seifert and Beheng, 2006). Additionally, environmental wind shear has been shown to have a role in determining the response of convective systems to aerosol, with increased aerosol loading invigorating convection under weak shear conditions and suppressing convection under strong shear in simulations performed with both bin (Fan et al., 2009) and bulk (Lebo and Morrison, 2014) microphysics schemes.

15 Whilst previous studies have focused either on the response to CCN or CDNC perturbations of a particular idealised (e.g. Thompson et al., 2004; Seifert and Beheng, 2006; Khain and Lynn, 2009; Lebo and Seinfeld, 2011; Morrison and Grabowski, 2011; Morrison, 2012), or real-data (e.g. Morrison and Pinto, 2005; van den Heever et al., 2006; Seifert et al., 2012) model configuration, or the sensitivity of a particular precipitation event to different microphysics schemes (e.g. Morrison and Pinto, 2006; Gallus Jr. and Pfeifer, 2008; Rajeevan et al., 2010; Jankov et al., 2011), fewer studies have investigated the response of

20 different microphysics schemes to perturbations in prescribed cloud parameters. Li et al. (2015) compared the response of two bulk microphysics schemes to two different CDNC values, but their study was limited to warm phase shallow convection. In simulations performed with bin microphysics, aerosols have been been shown to increase CDNC and reduce precipitation over eastern China (Fan et al., 2012) and to invigorate convection and suppress surface precipitation in idealised supercell cases (Khain and Lynn, 2009; Lebo et al., 2012), whilst equivalent simulations performed with bulk microphysics resulted in little

25 or no response to aerosol (Khain and Lynn, 2009; Lebo et al., 2012; Fan et al., 2012).

In this work we investigate the reponse of different bulk microphysics schemes to idealised aerosol perturbations, but unlike previous studies we further compare the response across several different cases of convection. We perform high-resolution convection-permitting simulations with the Weather Research and Forecast (WRF) model in three configurations: a real-data

30 simulation of deep convection in the Congo basin, an idealised supercell case, and a shallow convection large-eddy simulation (LES). In each case we compare hydrometeor development in two commonly used double-moment bulk schemes and investigate the response of each model configuration to CDNC perturbations. Our focus is not to provide a detailed process study of aerosol effects on convection per se (to do so in the context of multiple model configurations is beyond the scope of this paper), but rather to explore and identify uncertainty in the cloud and precipitation response to CDNC perturbations across

35 a range of model configurations. We acknowledge that, due to a lack of fully coupled aerosol-cloud processes (e.g. droplet

activation, wet deposition and buffering processes, Stevens and Feingold, 2009; Lee and Feingold, 2010; Seifert et al., 2012), the magnitude of response of bulk microphysics schemes to CDNC perturbations may exceed that in schemes that explicitly treat cloud processing of aerosol. Our goal therefore is to highlight the large uncertainty in cloud and precipitation responses in convection-permitting models, even between multiple configurations of the same widely used model.

2 Experimental design

We use the Advanced Research WRF version 3 (Skamarock et al., 2008) in three different configurations: a real-data simulation of deep convection over the Congo basin, an idealised supercell simulation, and a warm-rain shallow cumulus LES simulation. WRF is a nonhydrostatic, compressible, 3D atmospheric model. We use version 3.5 of WRF in the Congo basin and the idealised supercell simulations, but version 3.3.1 was utilised for the warm-rain LES simulation because the LES packages were only available for this version of the model at this time (Yamaguchi and Feingold, 2012). In order to keep the simulations as consistent with each other as possible, we therefore implement the versions of the microphysics schemes from WRF version 3.5 into version 3.3.1 of the model for the LES simulations. Each set of simulations is performed using two microphysics parameterisations, at three different prescribed CDNC values, resulting in a total of six simulations for each model configuration. The model configurations used in this study are summarised in Table 1.

2.1 Microphysics parameterisations

A significant body of work has shown that two-moment microphysics schemes generally represent cloud and precipitation characteristics more realistically than single-moment schemes (most recently Morrison et al., 2009; Wu and Petty, 2010; Weverberg et al., 2013, 2014; Igel et al., 2015), and thus our study is restricted to the comparison of two five-class, double-moment schemes commonly used in WRF and shown by Cintineo et al. (2014) to perform well against satellite observations of cloud in North America: that described by Morrison et al. (2005, 2009); Morrison and Milbrandt (2011) (hereafter Morrison, or abbreviated to MORR), and that described by Thompson et al. (2004, 2008) (hereafter Thompson, or THOM). Both schemes are two-moment in rain and ice (prognostic mass and number), while the Morrison scheme is also two-moment in snow and graupel. Both are single moment in cloud water: mass is the only prognostic liquid cloud variable, and CDNC is prescribed at a given value. Following the method used in many previous studies including those of Khain and Lynn (2009) and Morrison (2012), we prescribe CDNC values (in this study, at 100, 250 and 2500 cm^{-3}) as a proxy for CCN varying under conditions ranging from clean to highly polluted. The list of microphysics configurations tested and the abbreviations used to describe them are summarised in Table 2.

2.2 Model configurations

The real-data Congo simulations use a model domain covering a 2100 km × 2100 km region over the Congo Basin (Figure 1), chosen due to the high frequency of isolated deep convective systems occurring in the region and also due to the presence of strong sources of biomass burning aerosol. The model initial and boundary conditions were generated from ERA-Interim reanalysis (Dee et al., 2011), starting at 00:00 UTC on 1 August 2007. The simulation start date was chosen to coincide with the onset of the seasonal peak in precipitation (Washington et al., 2013) and the simulation was integrated for 10 days (with a timestep of 12 s) in order to identify the nature of the convection and its repsonse to CDNC perturbations over timescales greater than that of the lifecycle of any individual convective system. We use a horizontal grid length of 4 km and 30 vertical levels with the standard WRF stretched vertical grid. This gives a vertical grid spacing of about 100 m in the lower levels, with grid spacing increasing towards the upper levels. Although 30 vertical levels may seem relatively coarse, it has been shown in a previous study to be sufficient to reproduce observed cloud morphology and resolve the vertical structure of aerosol and precipitation and their interactions in this region (Gryspeerdt et al., 2015). Longwave and shortwave radiation in the simulations are parameterised by the RRTM (Mlawer et al., 1997) and Goddard (Chou and Suarez, 1994) schemes, respectively. Other physics parameterisations (other than the microphysics schemes previously discussed) are the MM5 Monin-Obukhov similarity surface layer scheme available in WRF (which uses stability functions and surface fluxes from Dyer and Hicks, 1970; Paulson, 1970; Webb, 1970; Beljaars, 1994), the NOAH land surface model (Ek and Mahrt, 1991) and the YSU boundary layer scheme (Hong et al., 2006), also shown by Cintineo et al. (2014) to perform well.

The idealised supercell setup follows the standard 3D idealised supercell case available as part of the WRF modelling system. Boundary conditions are open on all lateral boundaries, and the model top and surface are free-slip. For consistency with the Congo basin simulations, we use a horizontal grid length of 4 km. The model domain is 1600 km × 1600 km in the horizontal and, for consistency with the Congo simulations, also uses 30 vertical levels with a model lid at 20 km. A Rayleigh damper with damping coefficient of 0.003 s^{-1} is applied in the top 5 km of the model to prevent spurious wave reflection off the model top. Following the setup commonly used in idealised supercell studies (e.g. Morrison, 2012), surface energy fluxes, surface drag, Coriolis acceleration and radiative transfer are neglected for simplicity, and the subgrid-scale horizontal and vertical mixing is calculated with a prognostic turbulent kinetic energy scheme (Skamarock et al., 2008). The model is initialized as in the idealised quarter-circle supercell test case available in WRF, using the analytic sounding of Weisman and Klemp (1982, 1984) and the quartercircle supercell hodograph of Weisman and Rotunno (2000) with the shear extended to a height of 7 km. Convection is triggered using a thermal perturbation in the centre of the domain, with maximum perturbation potential temperature of 3 K centred at a height of 1.5 km and with horizontal and vertical radii of 10 km and 1.5 km, respectively. All simulations are integrated for 2 h with a timestep of 12 s (the same timestep used in the Congo simulations).

The warm-rain shallow cumulus setup deviates from the other simulations in that it follows the LES intercomparison guidelines for the Precipitating Shallow Cumulus Case 1 (van Zanten et al., 2011) of the Rain in Shallow Cumulus Over the Ocean

(RICO, Rauber et al., 2007) project and uses the RICO WRF LES package provided by Yamaguchi and Feingold (2012). The model domain is 12.8 km × 12.8 km × 4 km with a horizontal grid spacing of 100 m and uses 100 vertical levels, implying a vertical grid spacing of about 40 m. The lateral boundary conditions are doubly periodic. As in the idealised supercell simulations, surface energy fluxes, surface drag, Coriolis acceleration and radiative transfer are neglected for simplicity, and the subgrid-scale horizontal and vertical mixing is calculated with a prognostic TKE scheme. The surface conditions, wind and thermodynamic profiles, large-scale forcings and large-scale radiation, geostrophic wind, initial perturbations and translation velocity are prescribed following the RICO case guidelines (van Zanten et al., 2011). For consistency, we prescribe cloud droplet number concentrations at 100, 250 and 2500 cm^{-3} following the other simulations in our study, instead of the 70 cm^{-3} suggested for the standard RICO case. However, we also perform an extra simulation at 50 cm^{-3}. The simulations are integrated for 24 h with a timestep of 1 s.

3 Results

3.1 WRF Congo basin: real-data simulations

Maps of simulated outgoing longwave radiation (OLR) and surface precipitation at 0700 UTC on 7 August 2007 (7 days into the simulation) indicate that the cloud morphological and precipitation differences for different microphysics schemes are much greater than the cloud and precipitation response within each scheme to different CDNC values (Figure 1). In the CONGO-MORR simulations, low OLR values (indicating cold, high cloud) are distributed across the domain. Precipitation at this time occurs only in cloud north of 3° S, but there is a large band of non-precipitating cold cloud across the south of the domain. There is little discernable response of the morphology of the OLR and precipitation in the CONGO-MORR simulations to different CDNC values (Figs. 1a, 1b and 1c). In comparison, cold cloud in the CONGO-THOM simulations ocurrs mostly north of 3° S (Figs. 1d, 1e and 1f). Less cloud forms in CONGO-THOM compared to CONGO-MORR, and the cloud generally has greater OLR values than that in CONGO-MORR. Some non-precipitating cloud occurs south of 3° S in the CONGO-THOM simulations, but the band is significantly weaker and warmer than in CONGO-MORR. The differences at this snapshot are representative of differences that persist throughout the simulation. Frequency distributions of OLR over the entire 10-day simulation period show that CONGO-MORR has a much higher frequency of occurrence of colder, higher cloud (values about 120 W m^2) than CONGO-THOM (which increases in frequency slightly with increased CDNC), while CONGO-THOM has a much higher frequency of occurrence of warmer cloud (values about 270 W m^2) than CONGO-MORR (Figure 2a). When compared to observations of OLR from the Geostationary Earth Radiation Budget (GERB, Harries et al., 2005) over the same region and period, CONGO-THOM represents warm cloud more consistently with GERB than CONGO-MORR, despite overpredicting colder cloud somewhat, while CONGO-MORR overpredicts higher cloud and underpredicts warm cloud compared to the observations (Figure 2a). However, despite a poorer prediction of cloud radiative properties, CONGO-MORR predicts surface precipitation better than CONGO-THOM when compared to observations from the Tropical Rainfall Measuring Mission (TRMM, Huffman et al., 2007) merged product. Both schemes significantly overpredict surface precipitation

compared to observations from the TRMM 3B42 product (although the spatial patterns of precipitation are reasonably similar), however total accumulated surface precipitation over the 10-day simulation period is much greater in CONGO-THOM than CONGO-MORR (Figure 3). Further differences are seen when the distributions of precipitation rates are compared, with CONGO-THOM overpredicting and CONGO-MORR underpredicting the occurrence of low precipitation rates compared to

5 TRMM, CONGO-MORR overpredicting and CONGO-THOM underpredicting moderate rates, and CONGO-THOM overpredicting the frequency of occurrence of very high precipitation rates (Figure 2b). That CONGO-MORR overpredicts the frequency of moderate rain rates and CONGO-THOM overpredicts the frequency of very high rain rates likely explains why both schemes overpredict total accumulated surface rain compared to the observations. Additionally, the overprediction of the frequency of very high precipitation rates by CONGO-THOM is likely the reason that the total accumulated surface precipita-

10 tion is much greater in this scheme than in CONGO-MORR (Figure 3a,b).

Not only does the simulated cloud and precipitation morphology differ significantly between microphysics schemes irrespective of the CDNC values used in the comparison, zonal-mean vertical sections of mass mixing ratios of the different hydrometeor classes show significant differences in the hydrometero classes (due to microphysics) between CONGO-MORR

15 and CONGO-THOM (Figure 4). The most significant difference between the two microphysics schemes is that south of 3° S, CONGO-MORR produces a large amount of high ice cloud between 300 and 150 hPa (Figs. 4a, b, c). Analysis of these vertical sections at hourly intervals throughout the simulation in conjunction with hourly maps of OLR as in Figure 1 show that this upper-level ice is transported from the convective anvils in the north of the domain to the non-convective region in the south of the domain (not shown). In comparison, CONGO-THOM produces significantly less ice, with almost no ice visible

20 at this contour value (Figs. 4d, e, f). However, all three CONGO-THOM simulations form a large amount of non-precipitating low-level (950 to 850 hPa) liquid cloud south of 3° S. The bands of cloud seen south of 3° S in Figure 1 are therefore high ice cloud in the CONGO-MORR simulations and low liquid cloud in the CONGO-THOM simulations, illustrating not only a cloud morphological difference between the microphysics schemes but also a significant difference in the simulated hydrometeor classes and in the vertical distribution of hydrometeors. Even in the convective precipitating region in the north of the

25 domain, the simulated hydrometeor classes differ significantly between the microphysics configurations, with the CONGO-MORR simulations generating more ice and less liquid cloud (Figs. 4a, b, c) and the CONGO-THOM simulations producing less ice and more liquid cloud (Figs. 4d, e, f). Rain is confined to the convective region in the north in CONGO-THOM, while in CONGO-MORR it is also present at low levels in the non-convective southern region of the domain which is dominated by liquid cloud in CONGO-THOM. We explain the mechanisms behind these differences later, but here we highlight that it is

30 clear from Figure 4 that the differences in the simulated hydrometeors between microphysics schemes are much greater than the differences due to different levels of CDNC.

Because the partitioning of water into liquid and ice phases in the full-physics model configuration appears to depend strongly on the microphysics scheme, vertical sections of reflectivity occurrences derived from model hydrometeor fields

35 passed through the Quickbeam radar simulator (Haynes et al., 2007) are compared against an August reflectivity occurrence

climatology from the CloudSat 2B-GEOPROF product (Marchand et al., 2008) (Figure 5). The histograms are derived from the reflectivity fields thresholded to include all values greater than -20 dBZ. Note that the model data are from the 10-day simulation period only, sampled to the times nearest to each CloudSat overpass, whereas the satellite data show a mean of all overpasses that occur in August in the Congo basin domain over a 6 year period. With this limitation in mind, we use the satel-

5 lite radar data for a qualitative comparison only. The satellite data show that the model produces the highest reflectivities in the convective region in the north of the domain, where the highest reflectivities are also observed by the satellite radar (Figure 5, also in agreement with the TRMM precipitation observations (Figure 3). However, both CONGO-MORR and CONGO-THOM have a large positive bias in reflectivity compared to the observed climatology (Figure 5), indicative of limitations in the ability of both bulk microphysics schemes to represent the observed vertical cloud structure in this geographic region over this time

10 period. In general, CONGO-MORR has a much larger positive bias in reflectivity than CONGO-THOM (Figure 5). The Cloud-Sat observations show a small frequency of occurrence of reflectivities detected at altitudes of 10 to 15 km in the south of the domain, which is well-represented by CONGO-THOM and indicates the overproduction of ice in CONGO-MORR (Figure 5).

Differences in the simulated hydrometeor classes between the schemes persist throughout the simulation and are illus-

15 trated by domain-mean profiles of hydrometeor mass mixing ratios (Fig. 6). Most significantly, most of the condensate in the CONGO-M250 configuration is partitioned into the ice phase (Fig. 6a), whereas the CONGO-T250 profile is dominated by a large amount of liquid cloud mass between the near-surface and 750 hPa (Fig. 6b). The differences in cloud water mass between the schemes are very large: at 950 hPa (the altitude with the greatest liquid cloud mass in CONGO-T250, Figure 6), cloud water mass contents are about 140× greater in CONGO-T250. The liquid cloud mass is always greater in CONGO-T250

20 than CONGO-M250 (Fig. 6c), by several orders of magnitude at some levels, but despite this the liquid phase does not appear to drive differences in precipitation between the microphysics schemes: CONGO-M250 has about 4× more rain mass in the mid-levels and 2× more rain mass near the surface than CONGO-T250 (Figs. 6a and b). In the ice phase, CONGO-M250 has only slightly more snow mass than CONGO-T250 but up to 10× more graupel mass (Figs. 6a and b) and while ice is a significant hydrometeor at upper levels in CONGO-M250, CONGO-T250 has almost no cloud ice at all (Figs. 6a and b).

Not only does the partioning of ice amongst the hydrometeor classes differ between schemes, the response of the hydrometeors to CDNC perturbations also differs between schemes (Fig. 7). First note that the scale of the hydrometeor response to CDNC perturbations in the CONGO-MORR simulations is an order of magnitude smaller than the scale of the repsonse in the CONGO-THOM simulations. Liquid cloud mass appears insensitive to CDNC perturbations in the CONGO-MORR configu-

30 ration (Fig. 7a). Very weak decreases in near-surface rain mass may be evident under polluted conditions in CONGO-MORR, but this difference is on the order of 10^{-8} kg kg^{-1} (Fig. 7a). Nearly all of the hydrometeor response in CONGO-MORR occurs in the ice phase processes: graupel mass decreases under polluted conditions, while ice and snow mass increase (Fig. 7a). In contrast, the hydrometeor reponse to CDNC perturbations in the CONGO-THOM configuration is an order of magnitude greater than in CONGO-MORR and the dominant hydrometeor response to CDNC perturbations in CONGO-THOM occurs

35 in the liquid phase. Not only does the CONGO-THOM configuration generate a significant amount more liquid cloud than

the CONGO-MORR configuration (Figure 6c), but the liquid cloud mass increases under polluted conditions by an order of magnitude more than any other hydrometeor response (Fig. 7b). Rain mass decreases with increased CDNC (Fig. 7c), while snow production appears to shift to lower levels under polluted conditions, with a decrease in snow mass between 375 and 200 hPa and an increase in snow mass of about the same amount between 600 and 400 hPa (Fig. 7c).

3.2 WRF idealised supercell: ice phase processes

The results from the real-data Congo basin simulations indicate that the development of the simulated hydrometeor classes and the reponse of the hydrometeors to CDNC perturbations depend strongly on the choice of microphysics scheme. A few previous studies have focused on the response of real-data case studies to both microphysics scheme and CDNC response (e.g.

10 Fan et al., 2012, 2013; Li et al., 2015), but there is a larger body of literature that investigates the repsonse of idealised supercell simulations to CDNC (or CCN) perturbations (e.g. Seifert and Beheng, 2006; Khain and Lynn, 2009; Lebo and Seinfeld, 2011; Morrison, 2012). We therefore place our study in the wider context of the existing literature, simultaneously allowing us to explore the case-dependence of the deep convective response to aerosol effects, by investigating the reponse of a single isolated idealised supercell under both the MORR and THOM microphysics configurations to the same CDNC perturbations used in

15 our Congo simulations.

Figure 8 shows domain-mean hydrometeor profiles from the idealised supercell model configurations under 'moderately polluted' prescribed CDNC values of $250 \, \text{cm}^{-3}$. As in the Congo basin case, it is clear that the simulated hydrometeor classes differ significantly between schemes. However, we also see that the simulated hydrometeor classes differ between cases: the

20 difference in the simulated hydrometeor classes in the idealised supercell configuration is different from the difference in the real-data Congo basin configuration (Figure 8 compared to Figure 6). In contrast to the Congo basin configuration, both SUPER-MORR and SUPER-THOM configurations show similar behaviour in the liquid phase, producing similar profiles of liquid cloud mass and rain mass (Figures 8a and 8b), and instead the most significant differences occur in the ice phase. Graupel dominates as the frozen precipitating hydrometeor in the SUPER-M250 configuration, amounting to about 4× the snow

25 and ice masses at their peak amounts (Figure 8a). In contrast, snow is the dominant frozen precipitating hydrometeor in the SUPER-T250 configuration, amounting to about 1.5× the graupel mass at their peak amounts and virtually no ice present (Figure 8b). Although there is very little difference between the SUPER-MORR and SUPER-THOM configurations in the liquid phase (except for the SUPER-MORR configuration producing about $2 \times 10^{-7} \, \text{kg kg}^{-1}$ less rain mass at the surface than SUPER-THOM, Fig. 8c), the SUPER-MORR configuration forms significantly more ice, more graupel and less snow

30 than SUPER-THOM (highlighting that the partitioning of ice-phase hydrometeors into categories is very different, by design, in different microphysics schemes), and greater total quantities of frozen hydrometeors are present between 600 and about 150 hPa in SUPER-MORR compared to SUPER-THOM (Fig. 8c). This is a significant difference from the Congo real-data configuration, where the dominant contribution to the difference between the CONGO-MORR and CONGO-THOM configu-

rations came from the liquid cloud (Figure 6c).

In the real-data Congo basin configuration the response of the hydrometeors to CDNC perturbations was shown to differ between schemes (Fig. 7). This also occurs for the idealised, isolated supercell configuration (Figure 9). However, the hy-

5 drometeor response to CDNC perturbations also differs between the two cases. The SUPER-MORR case differs qualitatively from the CONGO-MORR case both in the altitudes at which the response occurs, and the sign of the response of some of the hydrometeors. In the SUPER-MORR configuration, cloud water mass increases under polluted conditions, and rain mass is suppressed at mid-levels (between 600 and 450 hPa) but shows negligible response at the surface (Fig. 9a). In the ice phase, cloud ice increases under polluted conditions in SUPER-MORR, while graupel and snow decrease (Fig. 9a). Similarly, the

10 hydrometeor response of the SUPER-THOM case to CDNC perturbations also differs in sign and in altitude to CONGO-THOM. In SUPER-THOM, cloud water mass increases and rain mass decreases under polluted conditions (Fig.9b), but unlike SUPER-MORR the decrease in rain is evident at the surface. Graupel mass decreases under polluted conditions in SUPER-THOM, similarly to SUPER-MORR but occurring over a much larger range of heights (Fig.9b), but unlike CONGO-THOM, which shows very little response to polluted conditions (Fig.7c). The dominant hydrometeor response to increased CDNC

15 perturbations in SUPER-THOM is an increase in snow mass between 550 and 150 hPa (Fig.9b). This is in contrast both to SUPER-MORR, where the dominant hydrometeor reponse occurred in the ice class (Fig.9a), and to CONGO-THOM, where the dominant hydrometeor reponse occurred in the liquid cloud (Fig.7b).

To further investigate the importance of the difference in microphysics representations and the difference in their response

20 to CDNC perturbations, Figure 10 includes the domain-mean total latent heating (sum of the latent heating from individual microphysical processes) contributions for each of the idealised supercell configurations. It can be seen that the choice of microphysics scheme can result in thermodynamic differences in the supercell system equal in magnitude to those arising from CDNC perturbations: between 500 and 250 hPa, the latent heating rate in the SUPER-M2500 configuration is almost identical to that in the SUPER-T250 configuration (solid red and dashed blue lines, Figure 10a). Thus, the magnitude and sign of the

25 difference in the latent heating rate between SUPER-M250 and SUPER-T250 (blue solid and dashed lines, Figure 10a) is the same as that between SUPER-M2500 and SUPER-M250 (red and blue solid lines), and likewise the magnitude and sign of the difference in the latent heating rate between SUPER-M2500 and SUPER-T2500 (red solid and dashed lines) is the same as that between SUPER-T2500 and SUPER-T250 (red and blue dashed lines). In general, the SUPER-THOM configuration has a much stronger thermodynamic response to CDNC perturbations than the SUPER-MORR configuration, with latent heating

30 rates consistently stronger throughout the atmosphere (Figure 10b). Overall, there is little evidence of convective invigoration (defined here as increases in upper-tropospheric heating, updraught strengths, cloud top height and surface precipitation) under increased CDNC values in either bulk microphysics scheme: although both schemes show increased latent heating in the upper troposphere and decreased heating at mid-levels under polluted conditions (Figure 10b), it has already been shown that there is no evidence of increased surface precipitation (Figure 9), and the upper tropospheric peak in latent heating can be seen to

35 correspond to an increase in ice (SUPER-M250) or snow (SUPER-T250) at these levels (Figure 9). Neither is there any sys-

3.3 WRF LES RICO: liquid-phase processes

5   The results presented in Sections 3.1 and 3.2 indicate that not only do the simulated hydrometeor classes differ between microphysics schemes and between cases, but that the hydrometeor response to CDNC perturbations also differs between microphysics schemes and between cases. The largest difference between the microphysics schemes in the real-data Congo basin simulations occurs in the liquid-phase hydrometeor development and response to CDNC. Making the assumption that the liquid phase is the first to respond to CDNC perturbations and the perturbation subsequently propagates to the ice phase, we

10   consider a case of precipitating shallow cumulus convection to investigate the liquid-phase differences between the schemes. Note that the 'baseline' hydrometeor profiles in Figure 11 show data from the configurations using a prescribed CDNC value of $100 \, cm^{-3}$ (rather than the baseline value of $250 \, cm^{-3}$ used in the Congo basin and idealised supercell deep convection cases in Figures 6 and 8), as this is more appropriate for a pristine marine environment. Even when we restrict our simulations to the liquid phase, differences in the simulated hydrometeor classes are evident. The dominant difference between the two schemes

15   in the RICO case is clearly in the rain profile, with RICO-T100 producing significantly more rain RICO-M100. Very little rain is present in the RICO-M100 configuration (Fig. 11a), whilst the RICO-T100 configuration produces a peak rain mass of about $10^{-6} \, kg \, kg^{-1}$ (Fig. 11b). The liquid cloud profile is similar in both schemes, with RICO-M100 forming more cloud mass than RICO-T100 between 805 and 775 hPa (Fig. 11c).

20   The response of the hydrometeors to CDNC perturbations also differs between schemes in the warm-rain RICO case (Fig. 12). In the RICO-MORR configuration, rain and cloud mass both decrease under polluted conditions, although the rain response is very weak (on the order of $10^{-8} \, kg \, kg^{-1}$) and the dominant response is a reduction in liquid cloud mass (Fig. 12a). In contrast, a reduction in rain mass is the dominant hydrometeor response under polluted conditions in the RICO-THOM configuration, and the decrease is nearly two orders of magnitude greater than that in RICO-MORR (Fig. 12b). The liquid cloud

25   response to polluted conditions in RICO-THOM is weaker than the rain response, but still stronger than the cloud response in RICO-MORR. Cloud mass decreases under polluted conditions between 935 and 825 hPa, but increases at higher levels (Fig. 12b). Note that once again, the response of the simulated hydrometeors to CDNC perturbations differs between cases: under polluted conditions, RICO-MORR exhibits a decrease in cloud and rain mass, while CONGO-MORR exhibits a decrease in rain mass with little reponse in the liquid cloud (Fig. 7a), and SUPER-MORR shows almost no liquid-phase response at

30   all (Fig. 9a). Likewise, RICO-THOM exhibits a decrease in rain and increase in cloud mass under polluted conditions, while CONGO-THOM exhibits similar behaviour (Fig. 7b) but SUPER-THOM shows a decrease in rain mass with little response in the liquid cloud (Fig. 9b).

To illustrate the difference in the strength of response of the schemes to CDNC, total accumulated surface rain is shown for each RICO configuration in Figure 13a, along with an extra configuration using a 'very pristine' CDNC value of 50 cm^{-3}, and a series of sensitivity tests that will be discussed later. The 50 cm^{-3} CDNC configuration has been added because even at a prescribed CDNC value of 100 cm^{-3} very little rain production occurs in the RICO-MORR configuration. Warm rain

5 formation differs strongly between schemes: very low CDNC values are required for the RICO-MORR configuration to produce any rain, whereas RICO-THOM produces significantly more rain at all CDNC values (Fig 13a). Even under very pristine conditions, the RICO-M50 configuration produces an order of magnitude less rain than RICO-T50 (Fig 13a). The different schemes also respond differently to CDNC perturbations. Rain production in RICO-MORR (which produces much less rain than RICO-THOM) shuts down very quickly as CDNC is increased: rain amounts are on the order of 10^2 mm at a CDNC value

10 of 50 cm^{-3}, 10^1 mm at a CDNC value of 100 cm^{-3}, 10^{-1} mm at a CDNC value of 250 cm^{-3}, and rain production ceases completely at a CDNC value of 2500 cm^{-3} (Fig 13a). In contrast, rain production persists for much larger CDNC values in RICO-THOM: rain amounts are on the order of 10^3 mm at CDNC values of 50 cm^{-3}, 10^2 mm at CDNC values of 100 cm^{-3}, 10^1 mm at CDNC values of 250 cm^{-3}, and while rain amounts are very low at CDNC values of 2500 cm^{-3} (on the order of 10^{-5} mm), rain production has not shut down completely (Fig 13a).

3.4 Sensitivity tests

Autoconversion is parameterised differently in the two microphysics schemes. The Thompson scheme follows an adaptation of Berry and Reinhardt (1974), while the Morrison scheme follows the method of Khairoutdinov and Kogan (2000). The autoconversion rates as a function of cloud water content for each of the model configurations are shown in Figure 14. Also

20 shown is the cloud water content (up to the mean plus 2 standard deviations) of each configuration . It is immediately clear that the threshold cloud liquid content for autoconversion in the Morrison scheme (solid lines) is significantly lower than that in the Thompson scheme (dashed lines), i.e. rain production can occur at much lower cloud liquid water contents in Morrison. However, small amounts of rain will be re-evapourated easily, and this may explain the rapid shutdown of rain production with increasing CDNC in the RICO-MORR case. It is also clear from the mean, (mean+1 standard deviation) and (mean+2 standard

25 deviations) cloud water content limits that rain production through autoconversion ought to be possible in all model configurations. However, despite the higher cloud water content threshold for autoconversion in the Thompson scheme, autoconversion rates are much greater once the threshold is reached, and liquid cloud is converted to rain much faster in Thompson than in Morrison. From Figure 14, it appears that the threshold for autoconversion is unlikely to be reached very often in any of the T2500 cases. In the deep convection configurations, rain can be generated through ice and mixed-phase processes, but in the

30 RICO warm-rain case this cannot occur. This explains why, compared to more pristine conditions, cloud mass increases in RICO-T2500 while rain mass decreases (Figure 12b).

Because Figure 14 indicates that the autoconversion threshold may be at least in part responsible for this response in the RICO-THOM case, we replace the autoconversion parameterisation in the Morrison scheme with that from the Thompson

scheme, and vice versa. We use the notation M100T to denote the Morrison microphysics scheme (at a CDNC value of 100 cm^{-3}) with Thompson autoconversion (that of Berry and Reinhardt, 1974), and T100M to denote the Thompson scheme with Morrison autoconversion (that of Khairoutdinov and Kogan, 2000). Differences in the domain-mean hydrometeor mixing ratio profiles for each of the autoconversion-swapped configurations in the RICO case are shown in Figure 15. It is immediately

5   clear that, in the warm-rain configuration, simply swapping the autoconversion treatment makes the hydrometeor development of the microphysics schemes much more like each other. The difference between the RICO-M100 configuration with the Morrison and Thompson autoconversion parameterisations (Fig. 15a) is quantitatively and qualitatively very similar to the difference between the RICO-M100 and RICO-T100 configurations (Fig. 11c). Likewise, the difference between the RICO-T100 configuration with the Morrison and Thompson autoconversion parameterisations (Fig. 15b) and finally the difference between

10   the RICO-T100 configuration with the Morrison autoconversion parameterisation and the RICO-M100 configuration with the Thompson autoconversion parameterisation (Fig. 15c) are also very similar to the difference between the RICO-M100 and RICO-T100 configurations (Fig. 11c).

Similarly, swapping the autoconversion parameterisations between the microphysics schemes in the RICO cases makes

15   the surface rain production of the microphysics schemes much more like each other. The accumulated surface rainfall in the RICO-M100T configuration looks much more similar to the surface rainfall in the RICO-T100 configuration than it does to the RICO-M100 configuration (Fig. 13a). Rain amounts are on the order of 10^2 mm in RICO-M100T and RICO-T100, whereas in RICO-M100 it is two orders of magnitude smaller (Fig. 13a). Likewise, the accumulated surface rainfall in the RICO-T100M configuration is of order 10^1 mm compared to 10^2 mm in the standard RICO-T100 case (Fig. 13a). To further test the impor-

20   tance of autoconversion in the liquid phase simulations, we first turn off autoconversion completely in the 100 cm^{-3} CDNC simulations, and then allow autoconversion to occur but prevent the accretion of cloud water by rain. By design, in the absence of ice processes, no precipitation occurs without autoconversion (Fig.13a, M100noAUTO and T100noAUTO). However, in the RICO 100 cm^{-3} CDNC liquid-phase configuration the Thompson scheme can produce surface rain from autoconversion alone (albeit two orders of magnitude less than when rain can also accrete cloud water, (Fig. 13a, T100noACCR and T100), showing

25   that autoconversion acts almost like a "seed" in this scheme, after which accretion takes over the rain production process. In contrast, zero surface precipitation is produced in RICO M100noACCR (Fig. 13a), showing that in this (liquid-phase only) configuration the Morrison scheme requires both the autoconversion of cloud droplets to rain and the accretion of rain by cloud droplets in order to produce surface precipitation.

30   Despite the significant effect of autoconversion in the liquid-phase simulations, changing the autoconversion parameterisation in the idealised supercell case has very little effect on the hydrometeor development (results not shown). This is unsurprising, as ice and mixed-phase processes will dominate this shear-driven deep convective environment. However, the Congo basin configurations show large differences between microphysics schemes in the partioning of water into liquid and ice phases (CONGO-THOM produces much more liquid cloud; CONGO-MORR produces much more ice). In the CONGO-THOM con-

35   figurations, the liquid-phase response to increased CDNC is also very similar to the RICO-THOM response (increased liquid

cloud mass and decreased rain mass, Fig. 7b). When the Thompson autoconversion treatment is implemented in the Morrison scheme, rain production in the southern half of the domain ceases in CONGO-M250T, and the liquid phase is instead represented by low-level cloud with structure similar to the CONGO-T250 configuration (Figure 16a, compared to Figure 4e). To test if radiative effects associated with large amounts of anvil ice drive or contribute to the differences in low cloud, we also

5 set the ice extinction coefficient to zero in both the longwave and shortwave radiation schemes in CONGO-M250. However, this has no effect on the low-cloud characteristics (Figure 16e compared to Figure 4b), and we therefore conclude that autoconversion of cloud water to rain is the factor dominating the absence of low-level cloud in the south of the domain in the CONGO-MORR simulations. In contrast, autoconversion is a less significant process in the CONGO-T250 configuration. Implementing the Morrison autoconversion treatment in the Thompson scheme has very little effect on the hydrometeor structure

10 in the CONGO-T250M configuration compared to the CONGO-M250 configuration (Figure 16b, compared to Figure 4b). As a final test, the autoconversion process is turned off in both of the microphysics schemes. This confirms that autoconversion dominates the lack of low cloud in CONGO-M250: the resulting liquid-phase hydrometeor structure (Figure 16c) is similar to both CONGO-T250 (Fig. 7b) and CONGO-M250T (Figure 16a). This also confirms that autoconversion is much less significant in the CONGO-THOM configurations: the bulk hydrometeor structure when autoconversion is turned off in CONGO-T250

15 (Figure 16d) is very similar to both CONGO-T250 (Fig. 7b) and CONGO-T250M (Figure 16b).

Our results show little impact of aerosol on precipitation in the Congo basin (Fig. 2b, Fig. 7), which is also seen when considering total accumulated surface precipitation (Fig. 13b), although CONGO-T2500 exhibits weak precipitation suppression under polluted conditions). This may be due to the longer duration of these simulations, performed over a larger domain,

20 allowing the interaction of many cloud systems rather than considering the lifetime of a single isolated cloud. However, we also see that although the representation of autoconversion has a significant effect on the vertical hydrometeor structure in the CONGO-M250 configurations (Fig. 4b, Fig. 16a and Fig. 16c), it has a much weaker effect on total surface precipitation (Fig. 13b, M250, T250, M250T, T250M, M250noAUTO and T250noAUTO). This is perhaps unsurprising, as the dominant contribution to the accumulated surface precipitation over the Congo domain will be from ice processes in the convective re-

25 gion and not from the liquid-phase cloud.

4 Discussion and Conclusions

In this study we used WRF coupled to two double-moment bulk microphysics schemes (Morrison et al., 2009; Thompson et al., 2008) to perform cloud system-resolving simulations of convection in the Congo basin, an idealised supercell, and a case

30 of shallow cumulus convection, and tested the sensitivity of the simulated hydrometeors and precipitation to the microphysics scheme and to CDNC perturbations. The simulations were performed to explore the uncertainty in cloud and precipitation development and response to aerosol perturbations in convection-permitting models that can arise from the microphysics rep-

resentation.

A key finding is that the simulated hydrometeor classes differ significantly between microphysics schemes. Another key finding is that the difference between the hydrometeor classes simulated by each microphysics scheme varies between cases of convection. The maximum relative difference in mass mixing ratio between each hydrometeor class in the M250 and T250 configurations for each case of convection is summarised in Table 3. Not only are the maximum differences in the domain-mean profiles of the hydrometeor classes simulated by each microphysics scheme on the order of at least tens of percent, but it is also clear that both the magnitude and sign of the difference varies between cases. In some cases, the magnitude of the difference is huge: most notably, in the Congo basin case the maximum difference in liquid cloud mass between the Morrison and Thompson schemes is on the order of 10^4 kg kg^{-1} more in Thompson (whereas in the RICO shallow cumulus case the maximum difference is on the order of 10^1 kg kg^{-1} less in Thompson). Likewise, in the RICO case the maximum difference in rain mass between the Morrison and Thompson schemes is on the order of 10^3 kg kg^{-1} more in Thompson (whereas in the Congo basin case the maximum difference is on the order of 10^1 kg kg^{-1} less in Thompson). Even for hydrometeors that have differences of the same order of magnitude, the sign of the difference can vary between cases. This result highlights the need for better observational constraints on mixed-phase and ice cloud microphysics and hydrometeors, and also perhaps the need for a shift in the development of microphysics parameterisations away from schemes which (somewhat arbitrarily) partition hydrometeors into separate categories.

In 10 day simulations of deep convection in the Congo basin in August 2007, we find that both the Morrison and Thompson schemes have a significant positive bias in cloud and surface precipitation compared to GERB and TRMM. This may be in part attributable to the positive moist bias in the Congo basin in the ERA-Interim reanalysis (used as boundary data for the Congo simulation) when compared to other reanalyses (Washington et al., 2013). Despite the positive cloud fraction bias in both schemes, we find that the Thompson scheme compares better than the Morrison scheme against observed cloud fractions, largely due to the overproduction of upper-level ice in the Morrison scheme. This is in agreement with Cintineo et al. (2014), who found that (despite the two schemes having different biases at different levels) the Thompson scheme outperformed the Morrison scheme overall against satellite observations of cloud in North America due to its more accurate upper-level cloud distribution, whereas the Morrison scheme had too much upper-level cloud through overproduction of ice. This could be attributable purely to the upper limits on ice number concentrations used in each scheme rather than to a more accurate description of ice-phase processes. The version of the Morrison scheme used in this study limits ice number concentrations to 0.3 cm^{-3}, whereas the Thompson scheme has an upper limit on ice number concentration a full order of magnitude smaller. However, we also find that despite a positive surface precipitation bias in both schemes, the Morrison scheme compares better to observations in this region over this period. This therefore makes it difficult to conclude that one scheme outperforms another overall, and suggests that when setting up a model configuration for research purposes, the choice of which scheme to use may best be guided as to whether surface precipitation or radiative effects are more important to the research question.

Another key finding is that the cloud morphological difference and the difference in the hydrometeors between different schemes is significantly larger than that due to CDNC perturbations. Although we have restricted our study to the comparison of double-moment bulk microphysics schemes, this result is consistent with Khain and Lynn (2009), who found that the difference in convection between a bulk and a bin scheme was much greater than the difference within each scheme to varying aerosol concentrations. We present the new result that the response of the hydrometeors to CDNC perturbations differs not just between schemes, but is also case-dependent for each scheme. The maximum relative difference in the domain-mean hydrometeor profiles between polluted and pristine CDNC values for each of the model configurations is summarised in Table 4. It is clear that both the magnitude and the sign of the reponse of each hydrometeor class to CDNC differs strongly not just between microphysics schemes, but also between cases. (Note that Table 4 shows relative amounts, and that the absolute difference in response to CDNC between each of the schemes and cases can also vary significantly).

Whilst it is not surprising that the different cases of convection differ in their hydrometeor development and in their response to polluted conditions, it is worth noting the magnitude and variation of the difference in response. A body of literature uses idealised model configurations to investigate storm-system response to aerosol loading (e.g. Seifert and Beheng, 2006; Khain and Lynn, 2009; Lebo and Seinfeld, 2011; Morrison, 2012) and to compare microphysics schemes (e.g. Lebo and Seinfeld, 2011). Our results highlight that the storm-system response in such a model configuration may not be representative of the response over larger spatiotemporal scales, supporting similar findings of larger-scale feedbacks and lifecycle-dependent responses in idealised (Morrison and Grabowski, 2011; Lee, 2012) and real-data (van den Heever et al., 2006) studies of aerosol–convection interations.

We emphasize that the nature of our study is highly idealised: neither microphysics scheme treats cloud processing of aerosol, and thus we expect that the magnitude of the cloud repsonse to polluted conditions found in our study provides an upper limit on that which would result if processes such as wet deposition or other buffering processes (e.g. Stevens and Feingold, 2009; Seifert and Beheng, 2006) were acccounted for. However, we note firstly that the highly different response of each of the schemes in each of the cases has significant implications for studies of aerosol effects on convection. Many aerosol–convection interaction studies compare the response to aerosol (or some proxy variable for aerosol) of a single model configuration of deep convection coupled to a single microphysics parameterisation (e.g. Lim et al., 2011). Considering the growing body of literature of aerosol–convection process interactions, our study shows that additional constraints are needed to allow us to reliably compare any studies that do not use exactly the same model and model configuration. Secondly, we note that although our results represent an upper limit on the uncertainties that exist between different configurations of the same model, the fact that the uncertainty exists highlights fundamental deficiencies in our understanding of cloud microphysical processes. Adding complexity to our models to represent processes that may dampen this uncertainty (e.g. wet deposition) without first addressing the uncertainties themselves would amount to making the model behave 'more correctly' simply by masking errors in the model physics.

We note that the vertical resolution used in this study is relatively coarse, and that a horizontal grid length of 4 km is at the limit of what may be considered as 'convection-permitting' (Bryan et al., 2003). However, we use this grid spacing for consistency with a previous study, where 10 km and 4 km grid lengths were shown to be sufficient to reproduce storm characteristics and aerosol–convection interactions in the Congo basin (Gryspeerdt et al., 2015). Previous studies have indicated sensitivity

5 of convection to horizontal grid spacing (e.g. Bryan and Morrison, 2012; Potvin and Flora, 2015) and also that the sensitivity to grid length can vary with microphysics scheme (Morrison et al., 2015b), although idealised ensemble studies of response to aerosol have shown that differences between polluted and pristine conditions were similar in simulations using horizontal grid lengths of 4 km, 2 km, and 0.5 km, respectively and were also relatively robust to domain size (Morrison and Grabowski, 2011). A full systematic study of the sensitivity of convective development and of aerosol indirect effects to horizontal and

10 vertical resolution, to domain size, and to microphysics parameterisation, is beyond the scope of the current study but remains a focus of ongoing work.

We find that the autoconversion representation alone is sufficient to explain most of the differences between microphysics schemes in the shallow cumulus case both in terms of their representation of cloud and precipitation (consistent with Li et al.,

15 2015) and also in terms of their response to CDNC. The dominant hydrometeor difference between the microphysics schemes in the RICO simulations occurs in the rain - a different result from both the Congo basin configuration (where the dominant difference occurs in the liquid cloud) and the idealised supercell configuration (where the dominant difference occurs in the graupel). We also find that autoconversion of cloud droplets to rain is the mechanism that prevents the formation (or persistence) of liquid-phase cloud in the south of the domain in the Congo basin simulations using the Morrison scheme. Modelling studies

20 and observations from RICO have found that warm rain formation can be explained by the observed aerosol distribution (Blyth et al., 2013). In the context of our findings, this strongly suggests that an accurate description of the autoconversion process in warm-rain regimes is fundamental not only to a realistic representation of cloud and precipitation, but also to its response to varying aerosol concentrations. Once again, this highlights the continuing need of our community for tight observational contraints on cloud and precipitation processes and their repsonse to aerosol.

The analysis provided here adds to the body of literature that explores the response of convection-permitting simulations to aerosol perturbations. Our study helps to bridge the gap in the literature between studies of a single precipitation event using multiple microphysics schemes and studies investigating the response of a single scheme to CDNC or CCN perturbations, and is the first such study to consider multiple cases of convection. This work highlights the large uncertainty in cloud morphology,

30 hydrometeor development and response to CDNC that can result not just from different microphysics representations but also in different cases of convection, and indicates the ongoing need for stronger observational constraints on hydrometeors and microphysical processes.

Acknowledgements. This work used the ARCHER UK National Supercomputing Service (http://www.archer.ac.uk). The research leading to these results has received funding from the European Research Council under the European Union's Seventh Framework Programme (FP7/2007–2013)/ERC grant agreement no. FP7- 280025 (ACCLAIM) and grant agreement no. FP7- 306284 (QUARERE). The Congo precipitation data used in this study were acquired as part of the Tropical Rainfall Measuring Mission (TRMM). The algorithms were developed by the TRMM Science Team. The data were processed by the TRMM Science Data and Information System (TSDIS) and the TRMM office; they are archived and distributed by the Goddard Distributed Active Archive Center. TRMM is an international project jointly sponsored by the Japan National Space Development Agency (NASDA) and the US National Aeronautics and Space Administration (NASA) Office of Earth Sciences. The Congo radiance data used in this study were acquired as part of the Geostationary Earth Radiation Budget Project. The CloudSat data was obtained from the CloudSat Data Processing Center. ERA-Interim data provided courtesy ECMWF. Thanks go to Zak Kipling and Laurent Labbouz (University of Oxford, UK) for helpful comments on this manuscript.

References

Albrecht, B.: Aerosols, Cloud Microphysics, and Fractional Cloudiness, Science, 245, 1227–1230, 1989.

Beljaars, A.: The parameterization of surface fluxes in large-scale models under free convection, Quarterly Journal of the Royal Meteorological Society, 121, 225–270, 1994.

5 Berry, E. and Reinhardt, R.: An Analysis of Cloud Drop Growth by Collection: Part I. Double Distributions, J. Atmos. Sci., 31, 1814—-1824, 1974.

Blyth, A., Lowenstein, J., Huang, Y., Cui, Z., Davies, S., and Carslaw, K.: The production of warm rain in shallowmaritime cumulus clouds, Quarterly Journal of the Royal Meteorological Society, 139, 20–31, 2013.

Bryan, G. and Morrison, H.: Sensitivity of a Simulated Squall Line to Horizontal Resolution and Parameterization of Microphysics, Mon.
10 Wea. Rev., 140, 202—-225, doi:http://dx.doi.org/10.1175/MWR-D-11-00046.1, 2012.

Bryan, G., Wyngaard, J., and Fritsch, J.: Resolution Requirements for the Simulation of Deep Moist Convection, Mon. Wea. Rev., 131, 2394—2416, doi:http://dx.doi.org/10.1175/1520-0493(2003)131<2394:RRFTSO>2.0.CO;2, 2003.

Chand, D., Wood, R., Ghan, S. J., Wang, M., Ovchinnikov, M., Rasch, P. J., Miller, S., Schichtel, B., and Moore, T.: Aerosol optical depth increase in partly cloudy conditions, Journal of Geophysical Research: Atmospheres, 117, 2012.

15 Chou, M.-D. and Suarez, M.: An efficient thermal infrared radiation parameterization for use in general circulation models, NASA Technical Memo, 1994.

Cintineo, R., Otkin, J. A., Xue, M., and Kong, F.: Evaluating the Performance of Planetary Boundary Layer and Cloud Microphysical Parameterization Schemes in Convection-Permitting Ensemble Forecasts Using Synthetic GOES-13 Satellite Observations, Monthly Weather Review, 142, 163–182, 2014.

20 Dee, D. P., Uppala, S. M., Simmons, A. J., Berrisford, P., Poli, P., Kobayashi, S., Andrae, U., Balmaseda, M. A., Balsamo, G., Bauer, P., Bechtold, P., Beljaars, A. C. M., van de Berg, L., Bidlot, J., Bormann, N., Delsol, C., Dragani, R., Fuentes, M., Geer, A. J., Haimberger, L., Healy, S. B., Hersbach, H., Hólm, E. V., Isaksen, L., Kållberg, P., Köhler, M., Matricardi, M., McNally, A. P., Monge-Sanz, B. M., Morcrette, J.-J., Park, B.-K., Peubey, C., de Rosnay, P., Tavolato, C., Thépaut, J.-N., and Vitart, F.: The ERA-Interim reanalysis: configuration and performance of the data assimilation system, Quarterly Journal of the Royal Meteorological Society, 137, 553–597, 2011.

25 Dyer, A. and Hicks, B.: Flux-gradient relationships in the constant flux layer, Quarterly Journal of the Royal Meteorological Society, 96, 715–721, 1970.

Ek, M. and Mahrt, L.: SU 1-D PBL Model User's Guide. Version1.04, Department of Atmospheric Sciences, Oregon State University, 1991.

Fan, J., Yuan, T., Comstock, J. M., Ghan, S., Khain, A., Leung, L. R., Li, Z., Martins, V. J., and Ovchinnikov, M.: Dominant role by vertical wind shear in regulating aerosol effects on deep convective clouds, Journal of Geophysical Research: Atmospheres, 114, n/a–n/a, 2009.

30 Fan, J., Leung, L. R., Li, Z., Morrison, H., Chen, H., Zhou, Y., Qian, Y., and Wang, Y.: Aerosol impacts on clouds and precipitation in eastern China: Results from bin and bulk microphysics, Journal of Geophysical Research: Atmospheres, 117, 2012.

Fan, J., Leung, L. R., Rosenfeld, D., Chen, Q., Li, Z., Zhang, J., and Yan, H.: Microphysical effects determine macrophysical response for aerosol impacts on deep convective clouds, Proceedings of the National Academy of Sciences, 110, E4581–E4590, 2013.

Feingold, G., Stevens, B., Cotton, W., and Walko, R.: An explicit cloud microphysics/LES model designed to simulate the Twomey effect,
35 Atmospheric Research, 33, 207 – 233, 1994.

Gallus Jr., W. A. and Pfeifer, M.: Intercomparison of simulations using 5 WRF microphysical schemes with dual-Polarization data for a German squall line, Advances in Geosciences, 16, 109–116, doi:10.5194/adgeo-16-109-2008, http://www.adv-geosci.net/16/109/2008/, 2008.

Gryspeerdt, E., Stier, P., and Partridge, D. G.: Links between satellite-retrieved aerosol and precipitation, Atmospheric Chemistry and Physics, 14, 9677–9694, 2014.

Gryspeerdt, E., Stier, P., White, B. A., and Kipling, Z.: Wet scavenging limits the detection of aerosol effects on precipitation, Atmospheric Chemistry and Physics, 15, 7557–7570, doi:10.5194/acp-15-7557-2015, http://www.atmos-chem-phys.net/15/7557/2015/, 2015.

Harries, J., Russell, J., Hanafin, J., Brindley, H., Futyan, J., Rufus, J., Kellock, S., Matthews, G., Wrigley, R., Last, A., Mueller, J., Mossavati, R., Ashmall, J., Sawyer, E., Parker, D., Caldwell, M., Allan, P., Smith, A., Bates, M., Coan, B., Stewart, B., Lepine, D., Cornwall, L., Corney, D., Ricketts, M., Drummond, D., Smart, D., Cutler, R., Dewitte, S., Clerbaux, N., Gonzalez, L., Ipe, A., Bertrand, C., Joukoff, A., Crommelynck, D., Nelms, N., Llewellyn-Jones, D., Butcher, G., Smith, G., Szewczyk, Z., Mlynczak, P., Slingo, A., Allan, R., and Ringer, M.: The geostationary Earth Radiation Budget Project, BULLETIN OF THE AMERICAN METEOROLOGICAL SOCIETY, 86, 945–+, doi:10.1175/BAMS-86-7-945, 2005.

Harrington, J. Y., Sulia, K., and Morrison, H.: A Method for Adaptive Habit Prediction in Bulk Microphysical Models. Part I: Theoretical Development, Journal of the Atmospheric Sciences, 70, 349–364, 2013.

Haynes, J. M., Luo, Z., Stephens, G. L., Marchand, R. T., and Bodas-Salcedo, A.: A Multipurpose Radar Simulation Package: QuickBeam, Bulletin of the American Meteorological Society, 88, 1723–1727, doi:10.1175/BAMS-88-11-1723, 2007.

Hong, S.-Y., Noh, Y., and Dudhia, J.: A new vertical diffusion package with explicit treatment of entrainment processes, Mon. Wea. Rev., 134, 2318–2341, 2006.

Hong, S.-Y., Lim, K.-S. S., Kim, J.-H., Lim, J.-O. J., and Dudhia, J.: Sensitivity Study of Cloud-Resolving Convective Simulations with WRF Using Two Bulk Microphysical Parameterizations: Ice-Phase Microphysics versus Sedimentation Effects, Journal of Applied Meteorology and Climatology, 48, 61–76, 2009.

Huffman, G. J., Adler, R. F., Bolvin, D. T., Gu, G., Nelkin, E. J., Bowman, K. P., Hong, Y., Stocker, E. F., David, and Wolff, B.: The TRMM Multi-satellite Precipitation Analysis: Quasi-Global, Multi-Year, Combined-Sensor Precipitation Estimates at Fine Scale, J. Hydrometeor, pp. 38–55, 2007.

Igel, A., Igel, M., and van den Heever, S.: Make It a Double? Sobering Results from Simulations Using Single-Moment Microphysics Schemes, J. Atmos. Sci., 72, 910–925, doi:10.1175/JAS-D-14-0107.1, 2015.

Jankov, I., Grasso, L., Sengupta, M., Neiman, P., Zupanski, D., Zupanski, M., Lindsey, D., Hillger, D., Birkenheuer, D., Brummer, R., and Yuan, H.: An evaluation of five arw-wrf microphysics schemes using synthetic goes imagery for an atmospheric river event affecting the california coast, J. Hydrometeor, 12, 618—-633, doi:http://dx.doi.org/10.1175/2010JHM1282.1, 2011.

Jiang, H., Cotton, W., Pinto, J., Curry, J., and Weissbluth, M.: Cloud Resolving Simulations of Mixed-Phase Arctic Stratus Observed during BASE: Sensitivity to Concentration of Ice Crystals and Large-Scale Heat and Moisture Advection, J. Atmos. Sci., 57, 2105—-2117, doi:http://dx.doi.org/10.1175/1520-0469(2000)057<2105:CRSOMP>2.0.CO;2, 2000.

Kessler, E. I.: On the distribution and continuity of water substance in atmospheric circulations, Meteorological Monographs, 1969.

Khain, A. and Lynn, B.: Simulation of a supercell storm in clean and dirty atmosphere using weather research and forecast model with spectral bin microphysics, Journal of Geophysical Research: Atmospheres, 114, 2009.

Khain, A., Pokrovsky, A., Pinsky, M., Seifert, A., and Phillips, V.: Simulation of Effects of Atmospheric Aerosols on Deep Turbulent Convective Clouds Using a Spectral Microphysics Mixed-Phase Cumulus Cloud Model. Part I: Model Description and Possible Applications, J. Atmos. Sci., 61, 2963—-2982, 2004.

Khain, A., Rosenfeld, D., and Pokrovsky, A.: Aerosol impact on the dynamics and microphysics of deep convective clouds, Quarterly Journal of the Royal Meteorological Society, 131, 2639–2663, 2005.

Khain, A. P., Beheng, K. D., Heymsfield, A., Korolev, A., Krichak, S. O., Levin, Z., Pinsky, M., Phillips, V., Prabhakaran, T., Teller, A., van den Heever, S. C., and Yano, J.-I.: Representation of microphysical processes in cloud-resolving models: Spectral (bin) microphysics versus bulk parameterization, Reviews of Geophysics, 53, 247–322, doi:10.1002/2014RG000468, 2015.

Khairoutdinov, M. and Kogan, Y.: A New Cloud Physics Parameterization in a Large-Eddy Simulation Model of Marine Stratocumulus, Mon. Wea. Rev., 128, 229—-243, 2000.

Koren, I., Kaufman, Y. J., Rosenfeld, D., Remer, L. A., and Rudich, Y.: Aerosol invigoration and restructuring of Atlantic convective clouds, Geophysical Research Letters, 32, doi:10.1029/2005GL023187, 2005.

Lebo, Z. J. and Morrison, H.: Dynamical Effects of Aerosol Perturbations on Simulated Idealized Squall Lines, Monthly Weather Review, 142, 991–1009, 2014.

Lebo, Z. J. and Seinfeld, J. H.: Theoretical basis for convective invigoration due to increased aerosol concentration, Atmospheric Chemistry and Physics, 11, 5407–5429, 2011.

Lebo, Z. J., Morrison, H., and Seinfeld, J. H.: Are simulated aerosol-induced effects on deep convective clouds strongly dependent on saturation adjustment?, Atmospheric Chemistry and Physics, 12, 9941–9964, doi:10.5194/acp-12-9941-2012, 2012.

Lee, S.: Effect of aerosol on circulations and precipitation in deep convective clouds, J. Atmos. Sci., 69, 1957—-1974, 2012.

Lee, S.-S. and Feingold, G.: Precipitating cloud-system response to aerosol perturbations, Geophysical Research Letters, 37, 2010.

Li, Z., Zuidema, P., Zhu, P., and Morrison, H.: The Sensitivity of Simulated Shallow Cumulus Convection and Cold Pools to Microphysics, J. Atmos. Sci., 72, 3340–3355, 2015.

Lim, K.-S. S., Hong, S.-Y., Yum, S. S., Dudhia, J., and Klemp, J. B.: Aerosol effects on the development of a supercell storm in a double-moment bulk-cloud microphysics scheme, Journal of Geophysical Research: Atmospheres, 116, doi:10.1029/2010JD014128, d02204, 2011.

Lin, Y.-L., Farley, R., and Orville, H.: Bulk Parameterization of the Snow Field in a Cloud Model, J. Climate Appl. Meteor., 22, 1065—-1092, doi:http://dx.doi.org/10.1175/1520-0450(1983)022<1065:BPOTSF>2.0.CO;2, 1983.

Loftus, A. and Cotton, W.: Examination of {CCN} impacts on hail in a simulated supercell storm with triple-moment hail bulk microphysics, Atmospheric Research, 147–148, 183 – 204, doi:http://dx.doi.org/10.1016/j.atmosres.2014.04.017, 2014.

Marchand, R., Mace, G. G., Ackerman, T., and Stephens, G.: Hydrometeor Detection Using Cloudsat—An Earth-Orbiting 94-GHz Cloud Radar, Journal of Atmospheric and Oceanic Technology, 25, 519–533, doi:10.1175/2007JTECHA1006.1, 2008.

Mauger, G. S. and Norris, J. R.: Meteorological bias in satellite estimates of aerosol-cloud relationships, Geophysical Research Letters, 34, 2007.

McFarquhar, G. M., Zhang, H., Heymsfield, G., Halverson, J. B., Hood, R., Dudhia, J., and Jr., F. M.: Factors Affecting the Evolution of Hurricane Erin (2001) and the Distributions of Hydrometeors: Role of Microphysical Processes, Journal of the Atmospheric Sciences, 63, 127–150, 2006.

Meyers, M. P., Walko, R. L., Harrington, J. Y., and Cotton, W. R.: New {RAMS} cloud microphysics parameterization. Part {II}: The two-moment scheme, Atmospheric Research, 45, 3 – 39, doi:http://dx.doi.org/10.1016/S0169-8095(97)00018-5, 1997.

Milbrandt, J. A. and Yau, M. K.: A Multimoment Bulk Microphysics Parameterization. Part III: Control Simulation of a Hailstorm, Journal of the Atmospheric Sciences, 63, 3114–3136, doi:10.1175/JAS3816.1, 2006.

Mlawer, E., Taubman, S., Brown, P., Iacono, M., and Clough, S.: Radiative transfer for inhomogeneous atmospheres: RRTM, a validated correlated k-model for the longwave, Journal of Geophysical Research, 102, 1997.

5   Morrison, H.: On the robustness of aerosol effects on an idealized supercell storm simulated with a cloud system-resolving model, Atmos. Chem. Phys., 12, 7689–7705, doi:10.5194/acp-12-7689-2012, 2012.

Morrison, H. and Grabowski, W. W.: A Novel Approach for Representing Ice Microphysics in Models: Description and Tests Using a Kinematic Framework, Journal of the Atmospheric Sciences, 65, 1528–1548, 2008.

Morrison, H. and Grabowski, W. W.: Cloud-system resolving model simulations of aerosol indirect effects on tropical deep convection and

10   its thermodynamic environment, Atmospheric Chemistry and Physics, 11, 10503–10523, 2011.

Morrison, H. and Milbrandt, J.: Comparison of Two-Moment Bulk Microphysics Schemes in Idealized Supercell Thunderstorm Simulations, Mon. Wea. Rev., 139, 1103–1130, doi:10.1175/2010MWR3433.1, 2011.

Morrison, H. and Milbrandt, J. A.: Parameterization of Cloud Microphysics Based on the Prediction of Bulk Ice Particle Properties. Part I: Scheme Description and Idealized Tests, Journal of the Atmospheric Sciences, 72, 287–311, 2015.

15   Morrison, H. and Pinto, J.: Mesoscale Modeling of Springtime Arctic Mixed-Phase Stratiform Clouds Using a New Two-Moment Bulk Microphysics Scheme, J. Atmos. Sci., 62, 3683—-3704, doi:http://dx.doi.org/10.1175/JAS3564.1, 2005.

Morrison, H. and Pinto, J.: Intercomparison of Bulk Cloud Microphysics Schemes in Mesoscale Simulations of Springtime Arctic Mixed-Phase Stratiform Clouds, Mon. Wea. Rev., 134, 1880–190, doi:http://dx.doi.org/10.1175/MWR3154.1, 2006.

Morrison, H., Curry, J., and Khvorostyanov, V.: A new double-moment microphysics parameterization for application in cloud and climate

20   models. Part I: Description, J. Atmos. Sci., 62, 1665–1677, 2005.

Morrison, H., Thompson, G., and Tatarskii, V.: Impact of Cloud Microphysics on the Development of Trailing Stratiform Precipitation in a Simulated Squall Line: Comparison of One- and Two-Moment Schemes, Mon. Wea. Rev., 137, 991–1007, doi:10.1175/2008MWR2556.1, 2009.

Morrison, H., Milbrandt, J. A., Bryan, G. H., Ikeda, K., Tessendorf, S. A., and Thompson, G.: Parameterization of Cloud Microphysics Based

25   on the Prediction of Bulk Ice Particle Properties. Part II: Case Study Comparisons with Observations and Other Schemes, Journal of the Atmospheric Sciences, 72, 312–339, 2015a.

Morrison, H., Morales, A., and Villanueva-Birriel, C.: Concurrent Sensitivies of an Idealized Deep Convective Storm to Parameterization of Microphysics, Horizontal Grid Resolution, and Environmental Static Stability, Mon. Wea. Rev., 143, 2082—2104, doi:http://dx.doi.org/10.1175/MWR-D-14-00271.1, 2015b.

30   Noppel, H., Blahak, U., Seifert, A., and Beheng, K. D.: Simulations of a hailstorm and the impact of {CCN} using an advanced two-moment cloud microphysical scheme, Atmospheric Research, 96, 286 –301, 2010.

Paulson, C.: The mathematical representation of wind speed and temperature profiles in the unstable atmospheric surface layer, Journal of Applied Meteorology, 9, 857–861, 1970.

Potvin, C. and Flora, M.: Sensitivity of Idealized Supercell Simulations to Horizontal Grid Spacing: Implications for Warn-on-Forecast,

35   Mon. Wea. Rev., 143, 2998—-3024, doi:http://dx.doi.org/10.1175/MWR-D-14-00416.1, 2015.

Rajeevan, M., Kesarkar, A., Thampi, S. B., Rao, T., Radhakrishna, B., and Rajasekhar, M.: Sensitivity of {WRF} cloud microphysics to simulations of a severe thunderstorm event over Southeast India, Ann. Geophys., 28, 603—-619, 2010.

Rauber, R., Ochs, H. I., Di Girolamo, L., Göke, S., Snodgrass, E., Stevens, B., Knight, C., Jensen, J. B., Lenschow, D. H., Rilling, R. A., Rogers, D. C., Stith, J. L., Albrecht, B. A., Zuidema, P., Blyth, A. M., Fairall, C. W., Brewer, W. A., Tucker, S., Lasher-Trapp, S. G., Mayol-Bracero, O. L., Vali, G., Geerts, B., Anderson, J. R., Baker, B. A., Lawson, R. P., Bandy, A. R., Thornton, D. C., Burnet, E., Brenguier, J.-L., Gomes, L., Brown, P. R. A., Chuang, P., Cotton, W. R., Gerber, H., Heikes, B. G., Hudson, J. G., Kollias, P., Krueger, S. K., Nuijens, L., O'Sullivan, D. W., Siebesma, A. P., and Twohy, C. H.: Rain in shallow cumulus over the ocean: the RICO campaign, Bull. Amer. Meteor. Soc., 88, 1912–1928, 2007.

Rosenfeld, D., Lohmann, U., Raga, G., O'Dowd, C., Kulmala, M., Fuzzi, S., Reissell, A., and M.O., A.: Flood or Drought: How Do Aerosols Affect Precipitation?, Science, 321, 1309–1313, 2008.

Rutledge, S. and Hobbs, P.: The mesoscale and microscale structure and organisation of clouds and precipitation in midlatitude cyclones. VIII: A model for the seeder-feeder process in warm frontal rainbands., J. Atmos. Sci., 40, 1185–1206, 1983.

Seifert, A. and Beheng, K. D.: A two-moment cloud microphysics parameterization for mixed-phase clouds. Part 2: Maritime vs. continental deep convective storms, Meteorology and Atmospheric Physics, 92, 67–82, 2006.

Seifert, A., Köhler, C., and Beheng, K. D.: Aerosol-cloud-precipitation effects over Germany as simulated by a convective-scale numerical weather prediction model, Atmospheric Chemistry and Physics, 12, 709–725, 2012.

Skamarock, W., Klemp, J., Dudhia, J., Gill, D., Barker, D., Duda, M., Huang, X., Wang, W., and Powers, J.: A Description of the Advanced Research WRF Version 3 NCAR Technical Note June 2008, Tech. Rep. TN-475+STR, NCAR, National Center for Atmospheric Research, Box 3000, Boulder, Colorado 80307, USA, 2008.

Stevens, B. and Feingold, G.: Untangling aerosol effects on clouds and precipitation in a buffered system, Nature, 461, 607–613, 2009.

Stevens, B., Feingold, G., Cotton, W., and Walko, R.: Elements of the Microphysical Structure of Numerically Simulated Nonprecipitating Stratocumulus, J. Atmos. Sci., 53, 980—-1006, 1996.

Tao, W.-K., Li, X., Khain, A., Matsui, T., Lang, S., and Simpson, J.: Role of atmospheric aerosol concentration on deep convective precipitation: Cloud-resolving model simulations, Journal of Geophysical Research: Atmospheres, 112, 2007.

Tao, W.-K., Chen, J.-P., Li, Z., Wang, C., and Zhang, C.: Impact of aerosols on convective clouds and precipitation, Reviews of Geophysics, 50, 2012.

Thompson, G. and Eidhammer, T.: A Study of Aerosol Impacts on Clouds and Precipitation Development in a Large Winter Cyclone, Journal of the Atmospheric Sciences, 71, 3636–3658, 2014.

Thompson, G., Rasmussen, R., and Manning, K.: Explicit Forecasts of Winter Precipitation Using an Improved Bulk Microphysics Scheme. Part I: Description and Sensitivity Analysis, Mon. Wea. Rev., 132, 519–542, doi:10.1175/1520-0493(2004)132<0519:EFOWPU>2.0.CO;2, 2004.

Thompson, G., Field, P., Rasmussen, R., and Hall, W.: Explicit Forecasts of Winter Precipitation Using an Improved Bulk Microphysics Scheme. Part II: Implementation of a new snow parameterization, Mon. Wea. Rev., 136, 5095–5115, 2008.

van den Heever, S., Carrió, G., Cotton, W., DeMott, P., and Prenni, A.: Impacts of Nucleating Aerosol on Florida Storms. Part I: Mesoscale Simulations, J. Atmos. Sci., 63, 1752–1775, 2006.

van Zanten, M. C., Stevens, B., Nuijens, L., Siebesma, A. P., Ackerman, A. S., Burnet, F., Cheng, A., Couvreux, F., Jiang, H., Khairoutdinov, M., Kogan, Y., Lewellen, D. C., Mechem, D., Nakamura, K., Noda, A., Shipway, B. J., Slawinska, J., Wang, S., and Wyszogrodzki, A.: Controls on precipitation and cloudiness in simulations of trade-wind cumulus as observed during RICO, Journal of Advances in Modeling Earth Systems, 3, doi:10.1029/2011MS000056, http://dx.doi.org/10.1029/2011MS000056, m06001, 2011.

Table 1. List of model configurations

Model settings	Congo	Supercell	RICO LES
horizontal grid length (km)	4	4	0.1
number of grid points (W–E and S–N)	525	400	129
number of vertical levels	30	30	100
model top	5000 Pa	20 km	4 km
time step (s)	12	12	1
simulation length	10 days	2 hours	24 hours
LW radiation scheme	RRTM	-	-
SW radiation scheme	Goddard	-	-
PBL scheme	YSU	-	-

Washington, R., James, R., Pearce, H., Pokam, W., and Moufouma-Okia, W.: Congo Basin rainfall climatology: can we believe the climate models?, Phil. Trans. R. Soc. B, 368, 2013.

Webb, E.: Profile relationships: The log-linear range, and extension to strong stability, Quarterly Journal of the Royal Meteorological Society, 96, 67–90, 1970.

5 Weisman, M. and Klemp, J.: The Dependence of Numerically Simulated Convective Storms on Vertical Wind Shear and Buoyancy, Mon. Wea. Rev., 110, 504–520, 1982.

Weisman, M. and Klemp, J.: The structure and classification of numerically simulated convective storms in directionally varying wind shears, Mon. Wea. Rev., 112, 2479–2498, 1984.

Weisman, M. and Rotunno, R.: The use of vertical wind shear versus helicity in interpreting supercell dynamics, J. Atmos. Sci., 57, 10 1452–1472, 2000.

Weverberg, K. V., Vogelmann, A. M., Lin, W., Luke, E. P., Cialella, A., Minnis, P., Khaiyer, M., Boer, E. R., and Jensen, M. P.: The Role of Cloud Microphysics Parameterization in the Simulation of Mesoscale Convective System Clouds and Precipitation in the Tropical Western Pacific, Journal of the Atmospheric Sciences, 70, 1104–1128, 2013.

Weverberg, K. V., Goudenhoofdt, E., Blahak, U., Brisson, E., Demuzere, M., Marbaix, P., and van Ypersele, J.-P.: Comparison of one-moment 15 and two-moment bulk microphysics for high-resolution climate simulations of intense precipitation, Atmospheric Research, 147–148, 145 – 161, 2014.

Wu, L. and Petty, G. W.: Intercomparison of Bulk Microphysics Schemes in Model Simulations of Polar Lows, Monthly Weather Review, 138, 2211–2228, doi:10.1175/2010MWR3122.1, 2010.

Yamaguchi, T. and Feingold, G.: Technical note: Large-eddy simulation of cloudy boundary layer with the Advanced Research WRF model, 20 Journal of Advances in Modeling Earth Systems, 4, doi:10.1029/2012MS000164, http://dx.doi.org/10.1029/2012MS000164, m09003, 2012.

Zhang, J., Reid, J. S., and Holben, B. N.: An analysis of potential cloud artifacts in MODIS over ocean aerosol optical thickness products, Geophysical Research Letters, 32, 2005.
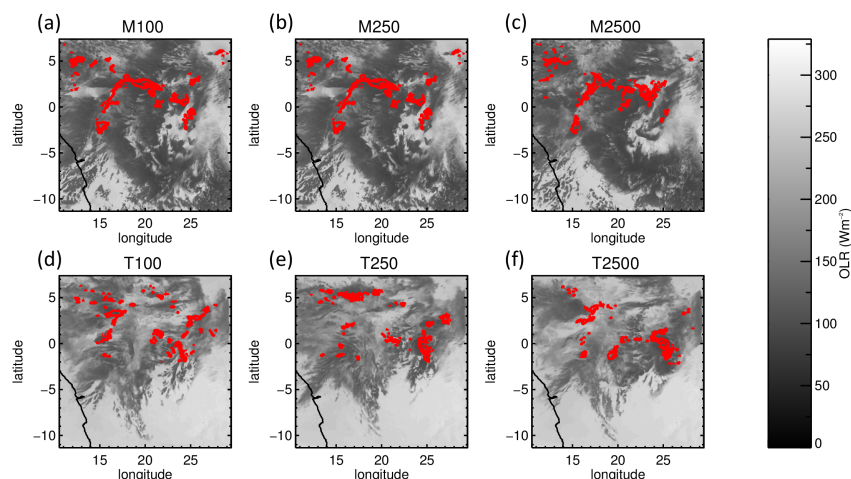
Figure 1. Congo case: Instantaneous outgoing longwave radiation (W m^2, greyscale) and 5 mm hr^{-1} surface precipitation rate (red contour) at 0700 UTC, 7 August 2007 in the Congo basin configuration. (a), (b) and (c) show CONGO-MORR simulations, (d), (e) and (f) show CONGO-THOM simulations. Prescribed CDNC values of 100, 250 and 2500 cm^{-3} are shown in (a, d), (b, e), and (c, f) respectively.
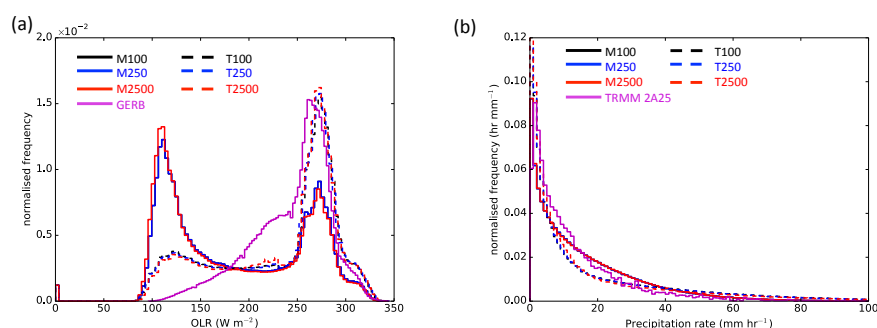
Figure 2. Congo case: (a) frequency distributions of OLR from the WRF simulations and observations from GERB over the period 01 to 10 August 2007 , (b) self-weighted precipitation rate distributions from the WRF simulations and observations from the ungridded TRMM 2A25 product, which has a similar spatial resolution to the 4 km model grid length.

Table 2. List of microphysics configurations tested, and the abbreviations used for each run

Prescribed CDNC	Congo MORR	Congo THOM	Supercell MORR	Supercell THOM	RICO MORR	RICO THOM
100 cm^{-3}	CONGO-M100	CONGO-T100	SUPER-M100	SUPER-T100	RICO-M100	RICO-T100
250 cm^{-3}	CONGO-M250	CONGO-T250	SUPER-M250	SUPER-T250	RICO-M250	RICO-T250
2500 cm^{-3}	CONGO-M2500	CONGO-T2500	SUPER-M2500	SUPER-T2500	RICO-M2500	RICO-T2500
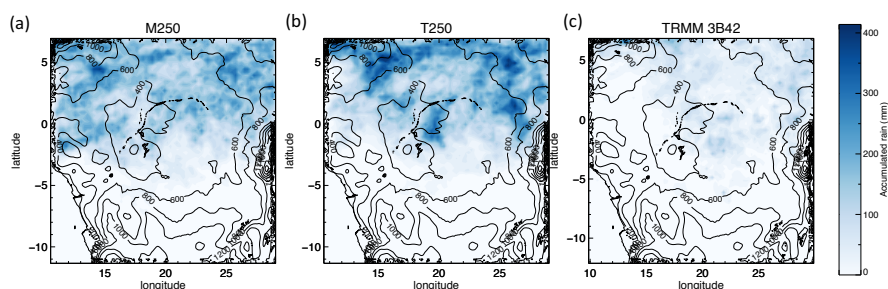
Figure 3. Congo case: accumulated surface precipitation (mm) from 01 to 10 August 2007 in the Congo basin, showing data from (a) CONGO-M250, (b) CONGO-T250 and (c) observations from the TRMM 3B42 gridded 3-hourly mean merged precipitation product. The simulation data shown in this Figure has been coarsened to the 0.25°spatial resolution of the TRMM product.
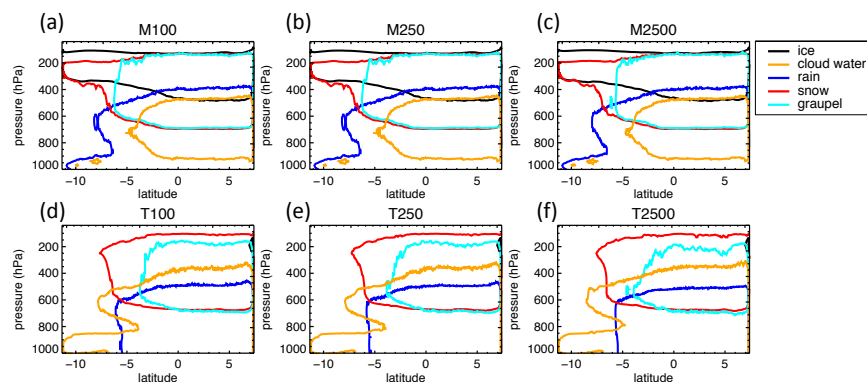
Figure 4. Congo case: Zonal mean vertical sections of hydrometeor classes (colour contours) from 01 to 10 August 2007. Hydrometeor mass mixing ratios are contoured at 10^{-6} kg kg^{-1}.
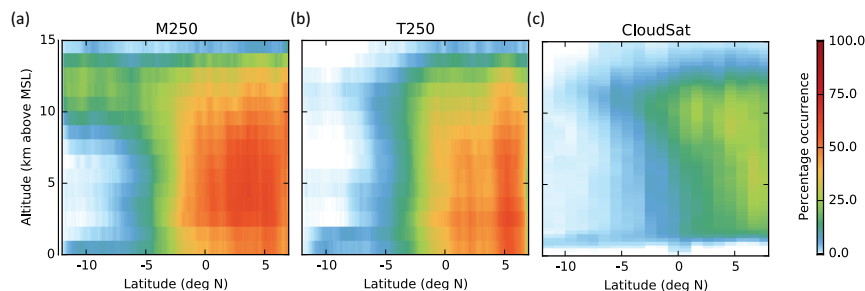
Figure 5. Congo case: 10-day histogram for the period 1–10 August 2007 of model reflectivities derived from hydrometeor fields passed through the Quickbeam radar simulator (Haynes et al., 2007), thresholded at values greater than -20 dBZ for (a) CONGO-M250, (b) CONGO-T250, and (c) equivalent histogram produced from climatology data from the CloudSat 2B-GEOPROF product from August 2006–2010 inclusive. In (a) and (b) the models have been sampled at the times of the nearest CloudSat overpasses.
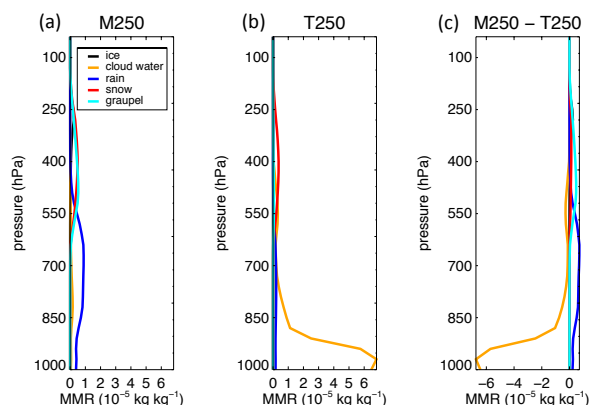
Figure 6. Congo case: Domain-mean vertical profiles of hydrometeor mass mixing ratios (MMR) averaged over the period 1–10 August 2007. (a) CONGO-M250, (b) CONGO-T250 and (c) the difference in the domain-mean hydrometeor mixing ratio profiles (CONGO-M250 minus CONGO-T250).
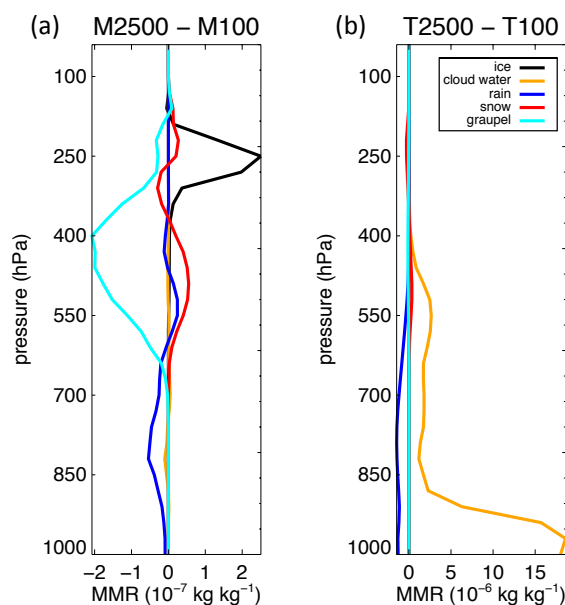
Figure 7. Congo case: Difference in the domain-mean hydrometeor mixing ratio profiles under polluted and pristine conditions averaged over the period 1–10 August 2007. (a) CONGO-M2500 minus CONGO-M100 and (b) CONGO-T2500 minus CONGO-T100. Note the difference in order of magnitude in the scale in (a) CONGO-MORR (10^{-7} kg kg^{-1}) compared to (b) CONGO-THOM (10^{-6} kg kg^{-1})
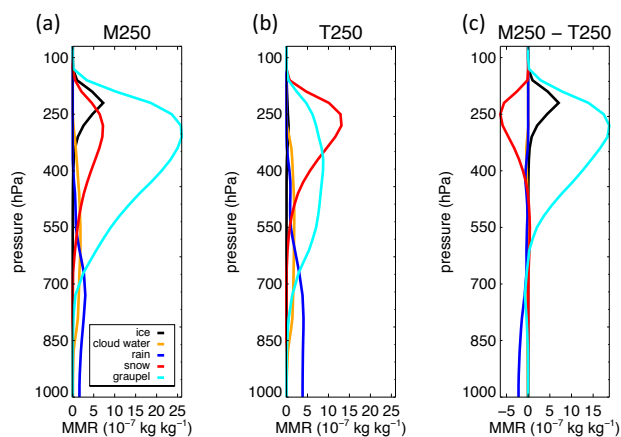
Figure 8. Idealised supercell: Domain-mean vertical profiles of hydrometeor mass mixing ratios (MMR), as Figure 6, averaged over the 2 h of the supercell simulation. (a) SUPER-M250, (b) SUPER-T250, (c) SUPER-M250 minus SUPER-T250.
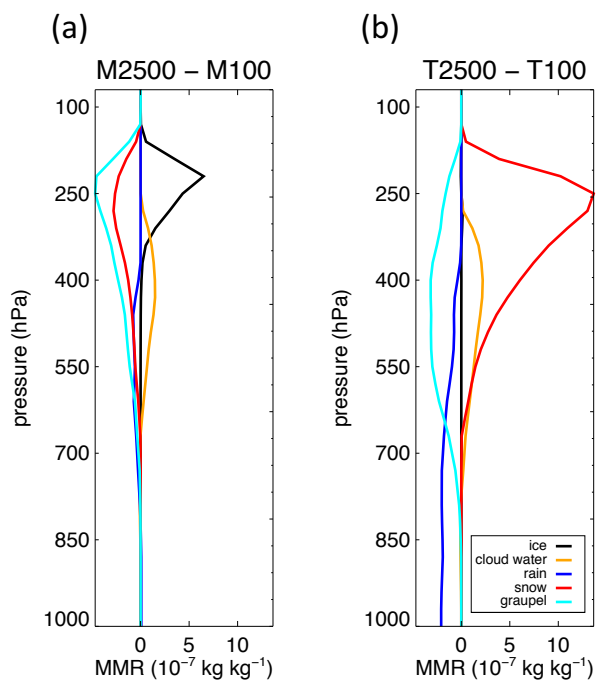
Figure 9. Idealised supercell: difference in the domain-mean hydrometeor mixing ratio profiles under polluted and pristine conditions, as Figure 7, averaged over the 2 h of the supercell simulation. (a) SUPER-M2500 minus SUPER-M100 and (b) SUPER-T2500 minus SUPER-T100.
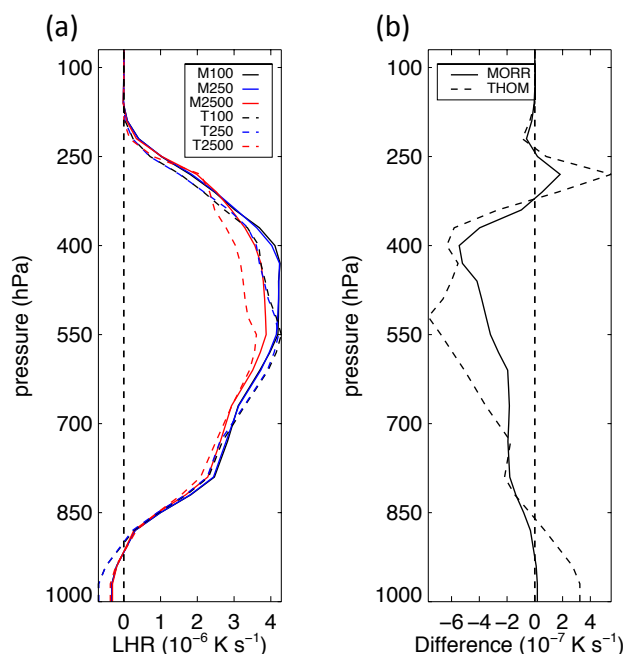
Figure 10. Idealised supercell: (a) Vertical profiles of domain-mean total latent heating rate (LHR) over the 2 h of the supercell simulation for SUPER-MORR and SUPER-THOM for CDNC values of 100, 250 and 2500 cm^{-3}. (b) Difference in the total latent heating contributions over the 2 h of the supercell simulation for SUPER-M2500 minus SUPER-M100 and SUPER-T2500 minus SUPER-T100.
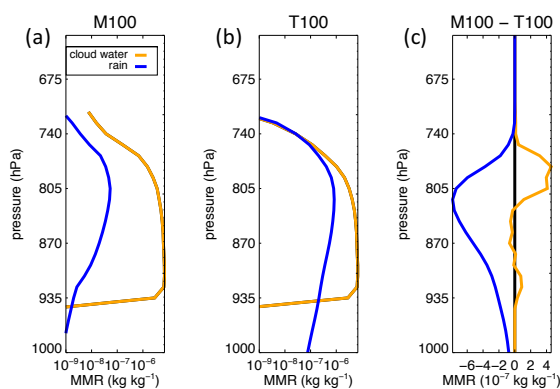
Figure 11. RICO case: Domain-mean vertical profiles of hydrometeor mass mixing ratios (MMR), as Figure 6, averaged over the 24 h of the RICO simulation. (a) RICO-M100, (b) RICO-T100, (c) RICO-M100 minus RICO-T100. Note that because the rain amounts are very small, especially in M100, (a) and (b) are shown with a logarithmic horizontal axis.
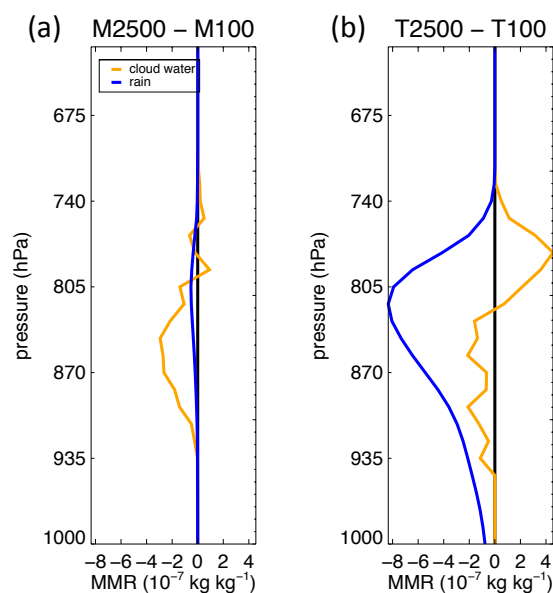
Figure 12. RICO case: difference in the domain-mean hydrometeor mixing ratio profiles under polluted and pristine conditions, as Figure 7, averaged over the 24 h of the RICO simulation. (a) RICO-M2500 minus RICO-M100, (b) RICO-T2500 minus RICO-T100

Table 3. Maximum relative difference of domain-mean hydrometeor mass mixing ratio profiles for the MORR and THOM schemes. The relative change in the hydrometeor mass mixing ratios are computed in each case for T250 compared to M250.

difference	CONGO	SUPERCELL	RICO
liquid cloud mass	-10900 %	-58.3 %	+17.0 %
ice mass	+98.7 %	+96.9 %	N/A
rain mass	+82.2 %	-138 %	-3830 %
snow mass	+40.8 %	-99.8 %	N/A
graupel mass	+91.6 %	+72.7 %	N/A
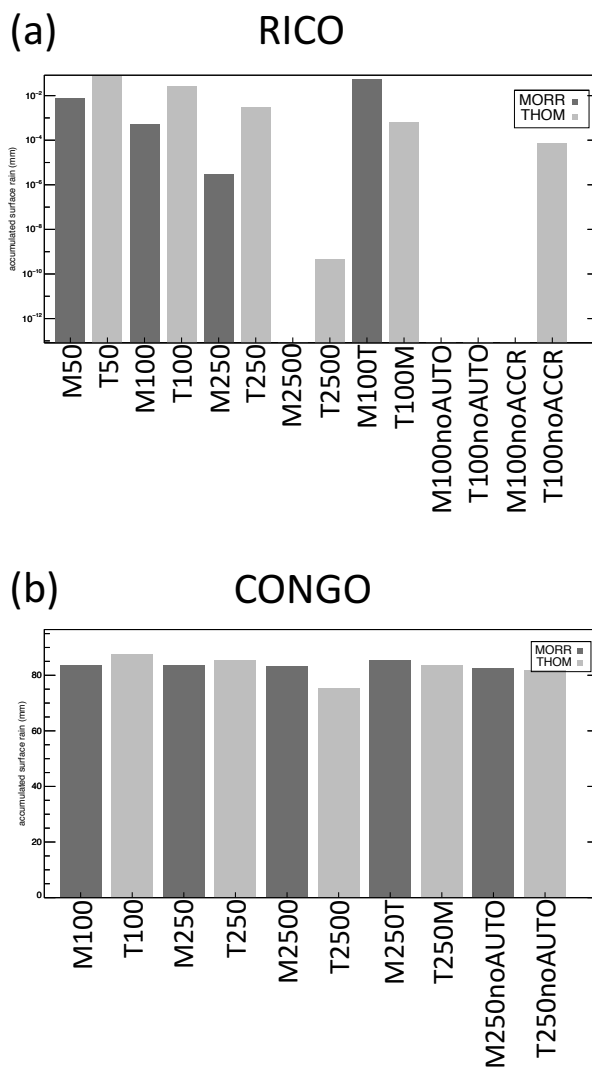
Figure 13. Total accumulated surface rain (mm) for each of the microphysics simulations, including a series of sensitivity simulations, for (a) RICO case, total after 24 h of simulation, (b) Congo case, total over the period 1–10 August 2007. Note that because the magnitude of the rain response to CDNC differs so strongly between the configurations in the RICO case, a logarithmic vertical axis is used in (a). The horizontal dashed line in (b) indicates the total precipitation from the TRMM 2A25 product over the same period.
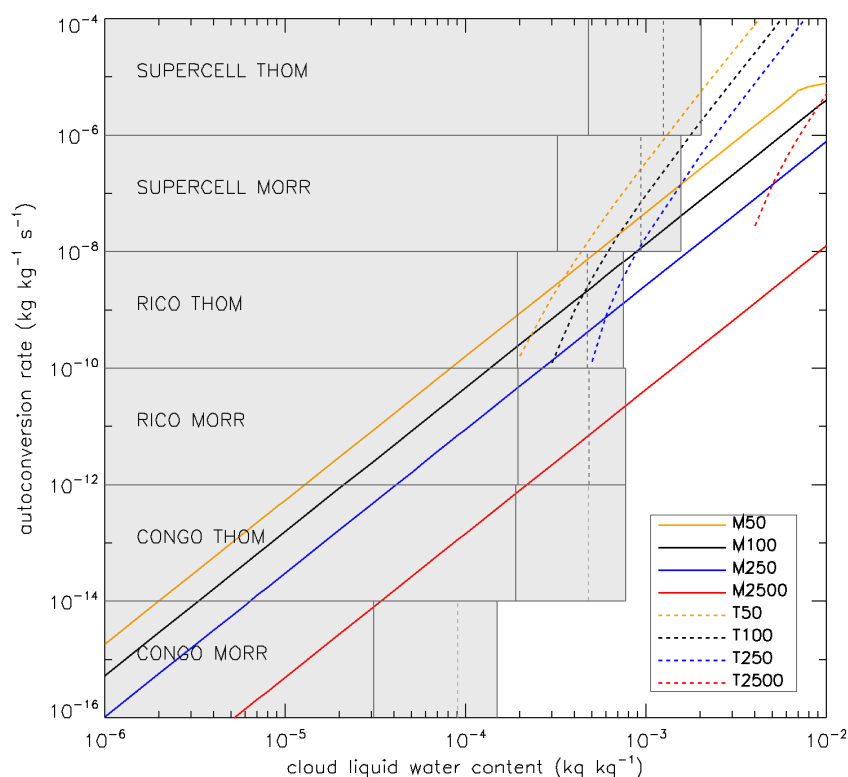
Figure 14. Autoconversion rate as a function of cloud water content for the MORR and THOM microphysics schemes (solid and dashed lines respectively) for super-pristine, pristine, moderately polluted and polluted conditions. Also shown are labelled grey bars showing the mean (solid vertical grey line) and 1 and 2 standard deviations (dashed vertical grey line and end of bar, respectively) cloud water content averaged over all prescribed CDNC configurations for each case (note that the variability in mean cloud water content with CDNC is significantly less than the variability due to microphysics scheme).
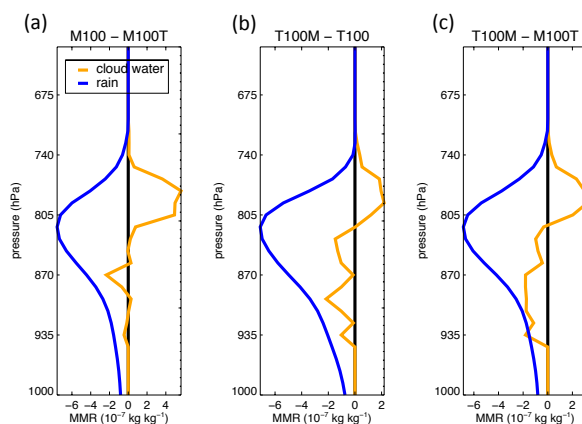
Figure 15. RICO case: Difference in the domain-mean vertical profiles of hydrometeor mass mixing ratios (MMR) between MORR and THOM, as Figure 11c, averaged over the 24 h of the RICO simulation for the configurations with the autoconversion treatment swapped between the microphysics schemes: (a) M100 minus M100T, (b) T100M minus T100, (c) T100M minus M100T

Table 4. Maximum relative difference of response of model configurations to polluted conditions. The relative change in the hydrometeor mass mixing ratios are computed in each case for CDNC values of $2500\,\mathrm{cm}^{-3}$ compared to $100\,\mathrm{cm}^{-3}$.

difference	CONGO-MORR	CONGO-THOM	SUPER-MORR	SUPER-THOM	RICO-MORR	RICO-THOM
liquid cloud mass	-0.59 %	+32.2 %	+146 %	+169 %	-5.21 %	+44.0 %
ice mass	+12.5 %	-5.61 %	+116 %	+29.7 %	N/A	N/A
rain mass	-0.67 %	-62.6 %	-93.7 %	-51.6 %	-100 %	-100 %
snow mass	+1.37 %	+13.8 %	-33.5 %	+109 %	N/A	N/A
graupel mass	-4.60 %	-29.9 %	-19.1 %	-36.7 %	N/A	N/A
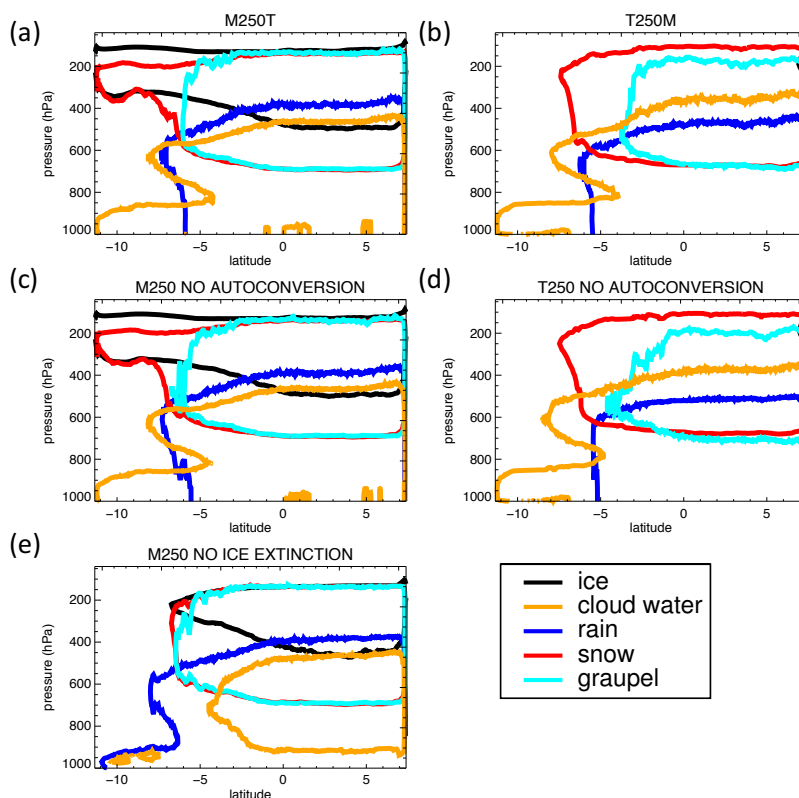
Figure 16. Congo case: Zonal mean vertical sections of hydrometeor classes (colour contours) from 01 to 10 August 2007, as Figure 4, but for the configurations with the autoconversion treatment swapped between the microphysics schemes, (a) CONGO-M250T and (b) CONGO-T250M, and for the configurations with (c) CONGO-M250 with autoconversion turned off, (d) CONGO-T250 with autoconversion turned off, (e) CONGO-M250 with the ice extinction coefficient set to zero in the longwave and shortwave radiation schemes. Hydrometeor mass mixing ratios are contoured at 10^{-6} kg kg^{-1}.